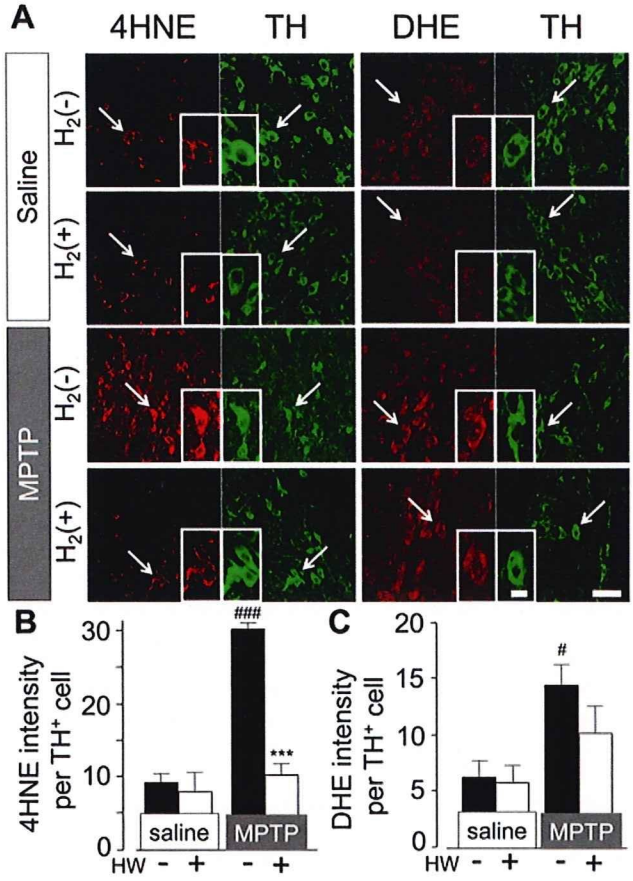

Figure 6. H_2 water reduced 4-HNE, but not DHE fluorescence in SN after MPTP administration. (A) Fluorescent images of 4-HNE, DHE, and TH in SN (n = 3~4). Mice treated with non-H_2 water or H_2/Mg water with injection of saline or MPTP. All samples were acquired 24 h after administration of saline or MPTP. Scale: 50 μm. (B, C) Quantification of 4-HNE (B) and DHE (C) intensity in TH-positive cells in SN. One-way ANOVA; $^{\#}P<0.05$, $^{\#\#\#}P<0.001$ compared to saline with non-H_2 water; $^{***}P<0.001$ compared to MPTP with non-H_2 water. Error bars represent mean ± SEM.
doi:10.1371/journal.pone.0007247.g006

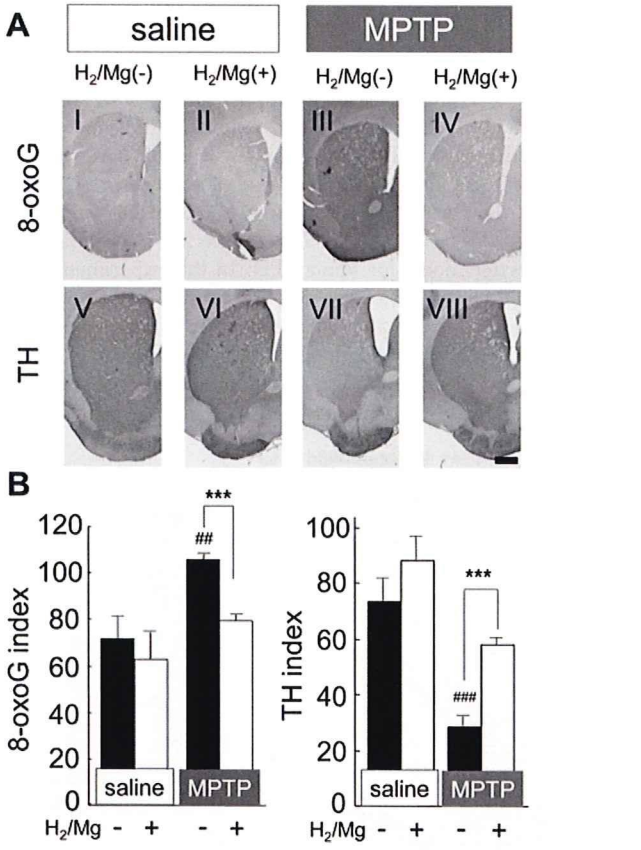

Figure 7. H_2 water decreased the accumulation of 8-oxoG in striatum after MPTP administration. (A) Acute administration of MPTP significantly increased the accumulation of mitochondrial 8-oxoG (I and III) and induced the loss of TH-positive neurons and fibers (V and VII). However, in mice drinking H_2/Mg water, no significant 8-oxoG accumulation (II and VI) nor TH-positive staining (VI and VIII) was observed. Brains were extirpated 24 h after administration of saline or MPTP. Scale: 500 μm. (B) Immunoreactive index for 8-oxoG and TH (n = 4 each). One-way ANOVA; $^{\#\#}P<0.01$ and $^{\#\#\#}P<0.001$ compared to saline with non-H_2 water; $^{***}P<0.001$, compared to MPTP with non-H_2 water. Error bars represent mean ± SEM.
doi:10.1371/journal.pone.0007247.g007

H_2 water reduced this accumulation to a level not significantly different from the control (Figure 7A, 7B). At 24 h after acute MPTP administration, microglia in the striatum were activated in mice drinking both H_2 and non-H_2 water (data not shown), and similarly in the SN 48 h after MPTP administration (Figure S1).

Discussion

This study shows that drinking water containing H_2 (H_2 water) attenuated the acute neurotoxic effects of MPTP on dopaminergic neurons. H_2 water was also effective on the behavioral impairment produced by chronic administration of MPTP, the major symptom of Parkinson's disease (PD). We found that low concentration of H_2 in drinking water, well below saturating concentrations, showed neuroprotective effects against the MPTP-induced loss of dopaminergic neurons and neuronal fibers in nigro-striatal pathway, and that this could be seen even after the start of the neurotoxic insult. H_2 water also reduced the amount of ROS-derived oxidative products such as 4-HNE and 8-oxoG, which would be primary causes of neuronal apoptosis in dopaminergic neurons. Thus, our study may pave the way toward a new neuroprotective strategy using H_2 water in PD patients.

PD is a progressive, degenerative disorder of the nervous system, meaning that it becomes increasingly disabling over time. It is a chronic, life-long condition. Various causes have been speculated: dopaminergic neurons can die or become damaged by infection, trauma, or toxins found in the environment, like MPTP. There may be also some genetic links. The impairments by all of these causes are generally related to varying degrees of oxidative stress [23]. Oxidative stress contributes to the cascade leading to dopamine cell degeneration in PD. Studies revealed that several biomarkers of oxidative damage are elevated in SN of PD brain [9]. Also, dopaminergic neurons may be a particularly fertile environment for the generation of ROS, as the metabolism of dopamine produces hydrogen peroxide and superoxide radicals, and auto-oxidation of dopamine produces dopamine-quinone, a molecule that damages proteins by reacting with cysteine residues [9,24].

Taking these reports into consideration, reducing oxidative stress or oxidative damage would become a potential way to prevent PD. H_2 acts as a therapeutic antioxidant by selectively reducing cytotoxic oxygen radicals [1–4,14,25,26], either by inhalation or consumption. Although inhalation of H_2 may act

more rapidly, it is not practical in daily life or suitable for continuous consumption. H_2 water is clearly more convenient, and fits well within a normal life-style. The most convenient form of H_2 water is H_2/Mg water. In our experiments, neither the alkalinity nor the magnesium had any effect but the small amounts of dissolved H_2 turned out to have significant neuroprotective and anti-oxidant effects.

As for the concentration of H_2, it was reported that H_2 dissolved in arterial blood was increased by the inhalation of H_2 in proportion to the concentration inhaled, from 0 to 4%, together with O_2 and N_2O; the amount of H_2 dissolved in venous blood was less than that in artery blood, suggesting that H_2 had been incorporated into tissues [1]. Recently it was also reported that the blood concentration of H_2 which was incorporated from the stomach using water with saturated H_2 was 5 μM [3]. We tried to measure the concentration of H_2 in rat striatum with cyclic voltammetry analysis using a H_2 electrode (Teflon-coated platinum electrode for the cerebral blood flow study, 200 μm in diameter) [27] inserted through a previously-mounted guide-cannula [28] (See Materials and Methods S2). We could detect the change in H_2 in the striatum during the inhalation of H_2 (Figure S2). It increased immediately when the rats started to inhale the H_2 gas and reached a plateau within 10 minutes (0.22 ppm; 110 μM), but decreased soon after stopping inhalation ($t_{1/2} = 343$ s; $n = 3$). However, we could not detect any change in H_2 concentration on instilling saturated H_2 water into the stomach in anesthetized rats or in free-moving rats drinking H_2-water. If there is 160 fold decrease in H_2 concentration between stomach and blood [3], there would be an even greater decrease between the H_2 concentration in drinking water (maximum 1.5 ppm) and that in striatal tissue. This suggests that the tissue H_2 concentration would be below detection level. Therefore, even though tissue H_2 would be expected to rise after drinking H_2 water, currently there is a technical problem in detecting such low levels.

In the PD model, ROS can be released from both cytosol and mitochondria of DA neuron [29–32]. Administration of MPTP causes its dysfunction via inhibition of complex I, which is associated with the electron transport chain [11]. Subsequent studies have identified abnormalities in complex I activity in PD [9,33]. Mitochondrial dysfunction causes massive production of ROS, especially $O_2\bullet^-$. At the nerve terminal of dopaminergic neuron in the striatum, where there are abundant mitochondria, more production of $O_2\bullet^-$ is predicted [9]. Furthermore, $O_2\bullet^-$ transforms into •OH by several steps including the Fenton reaction, which is catalyzed by ferrous iron (Fe^{2+}). Fe^{2+} can react with hydrogen peroxide (H_2O_2) (produced during oxidative deamination of dopamine) to generate •OH that can damage proteins, nucleic acids, and membrane phospholipids, leading to cellular degeneration [34–36]. We showed that a significant increase in markers characteristic of oxidative damage in the nigro-striatal pathway, such as 4-HNE, mitochondrial 8-oxoG, and DHE, occurred 24 h after MPTP administration. 4-HNE and 8-oxoG are well-known markers for oxidative insult mainly caused by •OH. 4-HNE was observed in membrane surface of TH-positive dopaminergic neuron in SN, and mitochondrial 8-oxoG was accumulated in the striatum over the same period (24 h after MPTP administration). It has been previously reported that mitochondrial 8-oxoG, the •OH -oxidative form of guanine and a marker of DNA damage, is accumulated the striatum of MPTP-injected mice [5]. However, hydrogen water significantly decreased the amount of 4-HNE in the SN and mitochondrial 8-oxoG in the striatum. This indicates that hydrogen acted by reducing the primary production of •OH in the nigro-striatal pathway.

A DHE fluorescence signal is detected when DHE and $O_2\bullet^-$ react and the oxidized DHE is incorporated into DNA. So, DHE is widely used for imaging intracellular $O_2\bullet^-$ both *in vitro* and *in vivo* [37–39]. During MPTP neurotoxicity, $O_2\bullet^-$ is released from not only neuronal mitochondria, but also by auto-oxidation of dopamine in dopaminergic neuron [40]. Also, NADPH oxidase in activated microglia is a source of $O_2\bullet^-$ in the nigro-striatal pathway [41]. However, in our experiments, we observed the production of $O_2\bullet^-$ at 24 h, before microglial activation. Although microglia are key players in the release of $O_2\bullet^-$, microglial NADPH activity is enhanced together with microglial activation and the peak of NADPH activity is only observed 48 h after administration of MPTP [42]. In our case, microglia was activated following the degeneration of dopaminergic neurons, not before, as shown in Figure S1. Although some microglia in the SN were activated in 24 h, we can conclude that DHE signals which we observed in 24 h after MPTP injection mostly reflected neuronal $O_2\bullet^-$ production in SN.

In a previous study, hydrogen reduced •OH but not other kinds of reactive oxygen/nitrogen species [1]. However, *in vivo*, there is little knowledge whether hydrogen shows selective reduction of ROS [4]. In our experiment, DHE intensity was not significantly reduced by hydrogen water in MPTP-treated mice, indicating that hydrogen water showed less or no reduction of $O_2\bullet^-$. This accords with the previous report that hydrogen showed a selective reduction of ROS [1]. On the othet hand, another study has shown that hydrogen water can reduce the amount of $O_2\bullet^-$ *in vivo* [4]. These opposite results may relate to the different concentrations of hydrogen in drinking water. Our hydrogen water contained a much lower amount of hydrogen than saturated hydrogen water, which may not be enough to reduce $O_2\bullet^-$.

We provided chronic MPTP administration model using osmotic minipump modifying the previous method. However, the number of TH-positive neurons in chronic MPTP model mice was more than acute MPTP model mice. Continuous MPTP infusion model caused less acute toxicity because the peak concentrations of MPP+ in striatum were lower [16]. Several reports indicated that the loss of dendritic processes in striatum and nigral TH-positive neurons' cell bodies were not permanent and recovery of striatal and nigral TH-immunoreactivity were observed after MPTP is eliminated systemically [42–44]. Such increases in TH-immunoreactivity may reflect sprouting of residual fibers [44] or the *de novo* appearance of TH-positive neurons in dopamine-depleted striatum [45–47], but more likely represent a compensatory mechanism for chronically reduced dopamine levels as suggested from post-mortem studies of PD brains [48]. Taking into consideration of these reports, we may conclude that the number of TH-positive neurons in chronic MPTP model does not decrease as much as in acute MPTP model because chronic recovery and damage of TH fiber occurred simultaneously in nigro-striatal pathway. Nevertheless, chronic administration induced behavioral impairment. This impairment may be due to degeneration of dopaminergic and noradrenergic neurons, i.e. loss of dopamine and norepinephrine, but not serotonin, from the target areas of the respective neurons. And what is more, chronic neurotoxicity induced formation of neuronal inclusion bodies and degeneration of catecholaminergic neurons, similar to the effects of chronic administration of rotenone which is also a mitochondrial complex I inhibitor [49–51]. Therefore, continuous mitochondrial inhibition may impair the ubiquitin proteasome system, which in turn recreates a disease state that mimics human PD better than acute mitochondrial inhibition.

Dopaminergic lesions induced by MPTP are commonly used to model of PD, and although MPTP effectively mimics the dopami-

nergic neuropathology of PD in mice, it fails to produce PD-like motor deficits [52]. Although continuous MPTP administration with an osmotic minipump mimics many features of the human disease [16], no significant effects in behavioral impairment except only open-field test showed significant change but not in other test such as rotarod test, tail suspension test, and ring test (data not shown). In acute PD model mice, age-related severity of dopaminergic neurodegeneration and motor dysfunction to MPTP neurotoxicity was reported. Although young (10 weeks) mice showed no mortality in either MPTP treatment, older (14–15 months) mice exhibited mortality from only two injections of MPTP during the experimental period [53]. Though the effects of H_2 water on behavioral response were not tested in older mice in the current study, our results raised a possibility that H_2 water may reduce the movement disorder in PD patients.

H_2 would be also useful for other diseases which are caused by oxidative stress. Already, H_2 has been found effective for not only ischemic injury but also hepatic damage and cognitive disease [1–3,23]. On the other hands, 8-oxoG is accumulated both in nuclear and mitochondrial genomes during aging [54], and dramatic increase in 8-oxoG accumulation was reported in patients with tumors [55] and other kinds of neurodegenerative disease such as PD [56], Alzheimer's disease [57] and amyotrophic lateral sclerosis [58]. Several experiments using genetic knockout mice revealed that the correlation between 8-oxoG accumulation and functional disorder of repair enzymes such as MTH1 [59], MUTYH [60], and OGG1 [61], suggesting that H_2 may also suppress tumorigenesis.

H_2 gas itself has a risk of flammability and explosion. However, drinking H_2 water would be much safer and easier, being more practical. In addition, the required concentration of H_2 in drinking water is not necessarily high. Our study also revealed that drinking H_2 water even after acute MPTP administration was effective as well. While there is no known way to prevent PD, the current studies strongly suggest that drinking H_2 water could reduce the risk of life style-related oxidative stress and related neurodegenerative diseases.

Materials and Methods

Hydrogen-containing water and its H_2 content

Hydrogen-containing water (H_2 water) was made by two ways. One way was by dissolving H_2 gas, produced by electrolysis of water (hand-made by Panasonic Electric Works Co., Ltd., Japan), directly into pure water. Another way was utilizing electrochemical reaction between magnesium and water (H_2O): $Mg+2H_2O \rightarrow Mg^{2+}+2OH^-+2H_2$. A magnesium stick composed of 90% Mg, 9% alminium and 1% zinc (6 mm diameter, 10 cm length, Nakagawa Metal, Japan) was surface-cleaned with 0.1 N acetic acid and dipped into pure water for about 1 minute. The maximum H_2 content with this method was about 0.08 ppm, measured with a hydrogen electrode (DH-35A, TOA DKK Co. Ltd., Japan). Electrolyzed H_2 water was also adjusted to have 0.08 ppm H_2 unless otherwise indicated.

pH of H_2 water and $Mg(OH)_2$ solution

The pH of H_2 water made by the chemical reaction with Mg was about 8.8 due to the formation of $Mg(OH)_2$, while the pH of pure water was 5.9. To investigate the effect of the alkaline solution (pH 8.8), $Mg(OH)_2$ (~80 μM) was added to pure water.

Treatment of mice with H_2 water

Animal protocols were approved by the Animal Care and Use Committee of Kyushu University. Male C57BL/6J (CLEA Japan Inc., Japan) mice of 8~12 weeks old were maintained on a 12:12 h light/dark cycle. H_2 water was made freshly each day and 40 ml was delivered in glass bottles with tight rubber caps per 4 mice for 8 h (4–12 p.m.). Unless otherwise indicated, mice were treated with H_2 or non-H_2 water for 7 days prior to MPTP administration. For MPTP chronic model, treatment with H_2 or non-H_2 water continued after MPTP administration.

Acute injection and continuous infusion of MPTP

For acute injection of MPTP, MPTP-HCl (20 mg/kg free base, SIGMA, USA) was administrated to mice intraperitoneally (i.p.) three times (2 h apart) and brains were extirpated under anesthesia 48 h after the last MPTP injection. MPTP was dissolved in 0.9% NaCl. For the continuous infusion of MPTP, an osmotic minipump (ALZET model 2004, USA) was transplanted subcutaneously, releasing either saline solution or MPTP solution at 45 mg/kg daily. After implantation, the incision was sutured, and disinfected with 70% ethanol every day. Twenty-eight days after the start of MPTP infusions, brains were extirpated under anesthesia. We checked that no solution was retained in the pump after the brain was removed.

Immunohistochemistry of tyrosine hydroxylase (TH)

TH-positive neurons were stained as described previously [5]. Brain sections (20 and 40 μm thick in SN and striatum, respectively) were incubated in blocking solution (Block Ace, Dainippon Pharmaceutical, Japan) for 30 min at room temperature, and then incubated with primary antibody (rabbit anti-TH antibody; 1:500, AB152, Chemicon, USA) in 10% Block Ace in PBS, at 4°C overnight. The rinsed sections were immersed in a solution of 3% H_2O_2 in methanol/PBS (1:1) for 30 min at room temperature, and then processed by the Vectastain ABC kit (Vector, USA) with secondary antibody (biotinylated anti-rabbit IgG, 1:200, Vector, USA). The peroxidase reaction product was detected using 3′3′-diaminobenzidine-tetrahydrochloride (DAB, Vector, USA). All sections were then washed in PBS, coverslipped, and analyzed by AxioSkop2 equipped with with a CCD camera, AxioCam (Carl Zeiss, Germany). The number of dopamine neurons in the SNpc was estimated by counting all TH-positive neurons of two hemispheres from six coronal sections (20 μm thick) per animal that were distributed every 100 μm along the rostral–caudate axis of the SN (−3.08 to −3.64 mm caudal to bregma) [62].

Microglial cells were stained as described in Materials and Methods S1 [References S1].

Stereological analysis of nigral Dopaminergic neuron

We performed stereological analysis using slightly modified method as described previously [63–65]. Coronal sections (30 μm thickness) were obtained through SNpc (−2.70 mm to −3.80 mm relative to bregma) on MICROM cryostat. Free-floating sections were incubated by Block Ace (Dainippon Pharmaceutics, Japan) for 30 min followed by incubation of primary antibody (anti-TH antibody, Chemicon, USA, 1:3000 in 10% Block Ace) for 2 days at 4°C. After the rinsed sections were immersed in a solution of 3% H_2O_2 in methanol/PBS (1: 1) for 10 min at room temperature, secondary antibody (biotinylated goat anti-rabbit IgG, 1:400, Vector, USA) were incubated for 2 h, and then were processed by Vectastain ABC kit (Vector, USA). The peroxidase reaction product was detected using 3′3′-diaminobenzidinetetrahydrochloride (DAB, Vector, USA). All sections were coverslipped with Glycergel Mounting Medium (Dako, Denmark).

For stereological counts, Stereo Investigator analysis software (Stereo Investigator 8, MicroBrightField Inc., USA) was used to

perform unbiased stereological counts of TH-immunoreactive cell bodies in the SNpc using optical fractionator method [66]. The boundary of SNpc was outlined under magnification of the 10x objective. Every third section (eight sections per brain) were obtained, and cells were counted with a 40x objective on a Nikon ECLIPSE 80i using a grid of 70×70 μm on a counting grid (75×100×12 μm) with 2 μm upper and lower guard zones. The absolute number of TH-positive neurons was directly calculated, and the Gundersen's coefficient of error in all samples were <0.07.

Labeling of intracellular superoxide *in vivo*

Intracellular superoxide levels were detected by quantification of fluorescence of the oxidation product of dihydroethidium (DHE, Molecular Probes, USA). Oxidation of DHE by superoxide converts DHE, which exhibits weak blue fluorescence, to an ethidium derivative (oxy-Et) that exhibits peak fluorescence in the rhodamine spectrum (excitation 480 nm, emission 567–586 nm) [20]. DHE, which is cell permeant, enters the cell and, after oxidation, binds to DNA with a small shift in its emission spectrum to 567 nm. DHE has increased specificity for superoxide compared with other dyes which are more general reactive oxygen species probes. DHE solution (200 μl; 1 mg/ml in PBS) was administrated intravenously 5 h before extirpating brain. Brains were sliced into 40 μm thicknesses using a cryostat and free-floating sections were obtained from the part of SN, as mentioned above in TH immunohistochemistry.

For immunofluorescent staining of TH, sections were incubated with Block Ace for 30 min at room temperature. The brain sections were incubated overnight at 4°C with primary antibody, rabbit anti-TH antibody (chemicon, 1:1000), and incubated for 4 h with Alexa fluor 488 goat anti-rabbit IgG (Molecular Probes, 1:500, USA) at room temperature. Every treatment was followed by washing three times for 5 min with PBS. Sections were mounted in the permafluor aqueous mounting medium (Thermo, Japan) and were analyzed with a confocal laser scanning microscope (LSM510META, Carl Zeiss, Germany).

Fluorescent labeling of 4-hydroxynonenal in SNpc

For detection of cellular lipid peroxide, we stained 4-hydroxynonenal (4-HNE). Briefly, free-floating sections were obtained from the part of SN, and incubated with primary antibody overnight following to the incubation with Block Ace. Then, sections were incubated with biotinylated anti-mouse IgG (Jackson, USA, 1:400), followed by streptavidin Alexa 594 (Molecular Probes, USA, 1:1000). After staining of 4-HNE, TH was stained as described above.

Quantitative analysis of DHE and 4-HNE fluorescent signal

All samples were analyzed with a confocal laser scanning microscope (LSM510META, Carl Zeiss, Germany). For each slice 10 series of z-stack images corresponding to 2 μm on the z-axis were obtained and projected using LSM image browser (Carl Zeiss, Germany). For quantification of fluorescent intensity of DHE and 4-HNE, all images were converted to grayscale, and the average of pixel intensity of each cell was measured using Adobe Photoshop CS3 (Adobe Systems). Over 60 cells which were merged with TH immunofluorescence were observed per animal and mean value of intensity/cell/animal was calculated in each group.

Immunohistochemistry of 8-oxoguanine in striatum

The method of staining 8-oxoG in mitochondrial DNA was described previously [5,22]. To eliminate cellular RNA, the sections were incubated in 10 mM Tris-HCl (pH 7.5), 15 mM NaCl containing DNase-free RNase (5 mg/ml of heat-incubated RNase A, Sigma, USA) for 60 min at 37°C. In this condition, nuclear DNA is not denatured at all, therefore the anti-8-oxoG antibody cannot access to 8-oxoG residues buried in the intact chromatin in nuclei, while the antibody easily accesses to 8-oxoG residues in mitochondrial DNA which does not have a tight chromatin structure. To detect 8-oxoG in nuclear DNA, section has to be subjected to pre-treatment with 2N HCl for 1 h at room temperature, which allows an efficient denaturation of nuclear chromatin but an extensive degradation of mitochondrial DNA [22]. Free-floating sections pre-treated were incubated in Block Ace, for 30 min at room temperature, and then were incubated with primary antibody (N45.1 mAb 1:100, Japan Institute for the Control of Aging, Japan) in 10% Block Ace, at 4°C overnight. The rinsed sections were immersed in a solution of 3% H_2O_2 in methanol/PBS (1: 1) for 15 min at room temperature, and then were processed by Vectastain ABC kit with a biotinylated secondary antibody, and the peroxidase reaction product was detected using DAB. Digital images were acquired using Axioskop2 plus equipped with a CCD camera, AxioCam. All sections from each experimental animal and group to be compared were processed in parallel.

Quantitative morphometric analysis of 8-oxoG

All acquired digital images were processed uniformly, as described previously [5], at a threshold in a gray scale mode to subtract any background corresponding to the area without tissue, and the optical density (OD) of each immunoreactive area was calculated by Adobe Photoshop version 7.0 (Adobe Systems). From each individual animal, five representative sections were measured and the mean OD was calculated as an immunoreactivity index for each animals. All quantitative analyses were performed by an individual unaware of the experimental treatments.

Open-field test for continuous MPTP infusion model mice

Before and 28 days after osmotic pumps were implanted, open-field tests were performed between 9 and 12 AM. A round open field with 60 cm in base diameter and 90 cm in upper diameter, surrounded by a 50 cm-high wall was used. During observation, a 100 W lamp-light was placed 80 cm above the field. Each mouse was put at the center of the field and the movements were recorded. Each mouse was tested for 3 min and the number of times they crossed a line drawn in the field was counted (modified from the method described previously [67]).

MPP+ measurement

HPLC-UV detection (wavelength, 295 nm) was used to measure 1-methyl-4-phenylpyridinium (MPP+, SIGMA, USA) levels in striatum using the method as described previously [68,69]. Mouse brains were subjected to be measured 1.5, 3, 6 h after MPTP was treated (n = 4). The standard solution of MPP+ (500 nM) was made by dilution of MPP+ stock solution (1 mM in 20% glycerol, 2.5% MeOH in pure water, pH 4.0 with H_3PO_4).

Statistical Analysis

All data represent mean±standard error of means (SEM). The data were compared with one-way ANOVA, followed by Bonferroni test. Values of $p < 0.05$ were considered statistically significant.

Supporting Information

Figure S1 Immunohistochemistry of microglia in substantia nigra. Mice drinking non-H_2 water (H_2(−)) or H_2 water (H_2(+)) were treated with saline or MPTP. Brains were obtained 24 h or 48 h after the last

injection of saline or MPTP. Microglial cells were immunostained with anti-Iba1 antibody (1:1000, WAKO). Scale: 50 μm.
Found at: doi:10.1371/journal.pone.0007247.s001 (3.97 MB TIF)

Figure S2 Representative concentration curve of H_2 in striatum. Anesthetized rats were inserted H_2 electrode to right striatum and currents were recorded by voltammetry. Rats started to inhale H_2 gas at 200 s after the start of recording, and stopped at 800 s.
Found at: doi:10.1371/journal.pone.0007247.s002 (0.39 MB TIF)

Materials and Methods S1
Found at: doi:10.1371/journal.pone.0007247.s003 (0.02 MB DOC)

Materials and Methods S2
Found at: doi:10.1371/journal.pone.0007247.s004 (0.02 MB DOC)

References S1
Found at: doi:10.1371/journal.pone.0007247.s005 (0.02 MB DOC)

Acknowledgments

We would like to thank Setsuko Kitamura, for her technical assistance, and Prof. David. A. Brown (UCL, UK) for discussion.

Author Contributions

Conceived and designed the experiments: YN MN. Performed the experiments: KF TS NY HY KS YY. Analyzed the data: KF TS HY YY. Contributed reagents/materials/analysis tools: MO HY MAK AT TK YT. Wrote the paper: KF YN MN. Undertook most of the experiments and wrote the manuscript: KF. Established MPTP-induced PD model mice: TS. Performed stereological analysis: NY. Contributed the generation of MPTP-induced PD model mice and behavioral analyses: HY HY. Contributed stereological analysis: KS. Contributed immunohistochemistry: MO YY MAK. Contributed to making H2 water: AT. Contributed H2 measurements: YK YT.

References

1. Ohsawa I, Ishikawa M, Takahashi K, Watanabe M, Nishimaki K, et al. (2007) Hydrogen acts as a therapeutic antioxidant by selectively reducing cytotoxic oxygen radicals. Nat Med 13: 688–694.
2. Cai J, Kang Z, Liu WW, Luo X, Qiang S, et al. (2008) Hydrogen therapy reduces apoptosis in neonatal hypoxia-ischemia rat model. Neurosci Lett 441: 167–172.
3. Nagata K, Nakashima-Kamimura N, Mikami T, Ohsawa I, Ohta S (2009) Consumption of molecular hydrogen prevents the stress-induced impairments in hippocampus-dependent learning tasks during chronic physical restraint in mice. Neuropsychopharmacology 34: 501–8.
4. Sato Y, Kajiyama S, Amano A, Kondo Y, Sasaki T, et al. (2008) Hydrogen-rich pure water prevents superoxide formation in brain slices of vitamin C-depleted SMP30/GNL knockout mice. Biochem Biophys Res Commun 375: 346–50.
5. Yamaguchi H, Kajitani K, Dan Y, Furuichi M, Ohno M, et al. (2006) MTH1, an oxidized purine nucleoside triphosphatase, protects the dopamine neurons from oxidative damage in nucleic acids caused by 1-methyl-4-phenyl-1,2,3,6-tetrahydropyridine. Cell Death Differ 13: 551–563.
6. Thomas B, Beal MF (2007) Parkinson's disease. Hum Mol Genetics 16: R183–194.
7. Schapira AH (2008) Mitochondria in the aetiology and pathogenesis of Parkinson's disease. Lancet Neurol 7: 97–109.
8. Olanow CW, Tatton WG (1999) Etiology and pathogenesis of Parkinson's disease. Annu Rev Neurosci 22: 123–144.
9. Dauer W, Przedborski S (2003) Parkinson's disease: mechanisms and models. Neuron 39: 889–909.
10. Javitch JA, D'Amato RJ, Strittmatter SM, Snyder SH (1985) Parkinsonism-inducing neurotoxin, N-methyl-4-phenyl-1,2,3,6-tetrahydropyridine: uptake of the metabolite N-methyl-4-phenylpyridine by dopamine neurons explains selective toxicity. Proc Natl Acad Sci U S A 82: 2173–2177.
11. Nicklas WJ, Youngster SK, Kindt MV, Heikkila RE (1987) MPTP, MPP^+ and Mitochondrial Function. Life Sci 40: 721–729.
12. Liang LP, Huang J, Fulton R, Day BJ, Patel M (2007) An orally active catalytic metalloporphyrin protects against 1-methyl-4-phenyl-1,2,3,6-tetrahydropyridine neurotoxicity in vivo. J Neurosci 27: 4326–4333.
13. Zhang W, Wang T, Qin L, Gao HM, Wilson B, et al. (2004) Neuroprotective effect of dextromethorphan in the MPTP Parkinson's disease model: role of NADPH oxidase. FASEB J 18: 589–591.
14. Yanagihara T, Arai K, Miyamae K, Sato B, Shudo T, et al. (2005) Electrolyzed hydrogen-saturated water for drinking use elicits an antioxidative effect: a feeding test with rats. Biosci Biotechnol Biochem 69: 1985–1987.
15. Langston JW (2002) The Impact of MPTP on Parkinson's Disease Research: Past, Present, and Future. In: Factor SA, Weiner WJ, eds. Parkinson's Disease. Diagnosis and Clinical Management: Demos Medical Publishing. xx p.
16. Fornai F, Schlüter OM, Lenzi P, Gesi M, Ruffoli R, et al. (2005) Parkinson-like syndrome induced by continuous MPTP infusion: convergent roles of the ubiquitin-proteasome system and alpha-synuclein. Proc Natl Acad Sci U S A 102: 3413–3418.
17. Stadler K, Bonini MG, Dallas S, Jiang J, Radi R, et al. (2008) Involvement of inducible nitric oxide synthase in hydroxyl radical-mediated lipid peroxidation in streptozotocin-induced diabetes. Free Radic Biol Med 45: 866–874.
18. Awasthi YC, Sharma R, Sharma A, Yadav S, Singhal SS, et al. (2008) Self-regulatory role of 4-hydroxynonenal in signaling for stress-induced programmed cell death. Free Radic Biol Med 45: 111–118.
19. Selley ML (1998) (E)-4-hydroxy-2-nonenal may be involved in the pathogenesis of Parkinson's disease. Free Radic Biol Med 25: 169–174.
20. Zhao H, Kalivendi S, Zhang H, Joseph J, Nithipatikom K, et al. (2003) Superoxide reacts with hydroethidine but forms a fluorescent product that is distinctly different from ethidium: potential implications in intracellular fluorescence detection of superoxide. Free Radic Biol Med 34: 1359–1368.
21. Oka S, Ohno M, Tsuchimoto D, Sakumi K, Furuichi M, et al. (2008) Two distinct pathways of cell death triggered by oxidative damage to nuclear and mitochondrial DNAs. EMBO J 27: 421–432.
22. Ohno M, Oka S, Nakabeppu Y (2009) Quantitative analysis of oxidized Guanine, 8-oxoguanine, in mitochondrial DNA by immunofluorescence method. Methods Mol Biol 554: 199–212.
23. Jenner P, Olanow CW (1996) Oxidative stress and the pathogenesis of Parkinson's disease. Neurology 47: S161–170.
24. Graham DG (1978) Oxidative pathways for catecholamines in the genesis of neuromelanin and cytotoxic quinones. Mol Pharmacol 14: 633–643.
25. Fukuda K, Asoh S, Ishikawa M, Yamamoto Y, Ohsawa I, et al. (2007) Inhalation of hydrogen gas suppresses hepatic injury caused by ischemia/reperfusion through reducing oxidative stress. Biochem Biophys Res Commun 361: 670–674.
26. Hayashida K, Sano M, Ohsawa I, Shinmura K, Tamaki K, et al. (2008) Inhalation of hydrogen gas reduces infarct size in the rat model of myocardial ischemia-reperfusion injury. Biochem Biophys Res Commun 373: 30–35.
27. Ooboshi H, Sadoshima S, Ibayashi S, Yao H, Uchimura H, et al. (1993) Isradipine attenuates the ischemia-induced release of dopamine in the striatum of the rat. Eur J Pharmacol 233: 165–168.
28. Katafuchi T, Oomura Y, Yoshimatsu H (1985) Single neuron activity in the rat lateral hypothalamus during 2-deoxy-D-glucose induced and natural feeding behavior. Brain Res 359: 1–9.
29. Przedborski S, Kostic V, Jackson-Lewis V, Naini AB, Simonetti S, et al. (1992) Transgenic mice with increased Cu/Zn-superoxide dismutase activity are resistant to N-methyl-4-phenyl-1,2,3,6-tetrahydropyridine-induced neurotoxicity. J Neurosci 12: 1658–1667.
30. Lotharius J, O'Malley KL (2000) The parkinsonism-inducing drug 1-methyl-4-phenylpyridinium triggers intracellular dopamine oxidation. A novel mechanism of toxicity. J Biol Chem 275: 38581–38588.
31. Hasegawa E, Takeshige K, Oishi T, Murai Y, Minakami S (1990) 1-Methyl-4-phenylpyridinium (MPP+) induces NADH-dependent superoxide formation and enhances NADH-dependent lipid peroxidation in bovine heart submitochondrial particles. Biochem Biophys Res Commun 170: 1049–1055.
32. Klivenyi P, St Clair D, Wermer M, Yen HC, Oberley T, Y et al. (1998) Manganese superoxide dismutase overexpression attenuates MPTP toxicity. Neurobiol Dis 5: 253–258.
33. Greenamyre JT, Sherer TB, Betarbet R, Panov AV (2001) Complex I and Parkinson's disease. IUBMB Life 52: 135–141.
34. Beal MF (1992) Does impairment of energy metabolism result in excitotoxic neuronal death in neurodegenerative illnesses? Ann Neurol 2: 119–130.
35. Gutteridge JM (1992) Iron and oxygen radicals in brain. Ann. Neurol 32: S16–21.
36. Kaur D, Yantiri F, Rajagopalan S, Kumar J, Mo JQ, et al. (2003) Genetic or pharmacological iron chelation prevents MPTP-induced neurotoxicity in vivo: a novel therapy for Parkinson's disease. Neuron 37: 899–909.
37. Behrens MM, Ali SS, Dao DN, Lucero J, Shekhtman G, et al. (2007) Ketamine-induced loss of phenotype of fast-spiking interneurons is mediated by NADPH-oxidase. Science 318: 1645–1647.
38. Robinson KM, Janes MS, Pehar M, Monette JS, Ross MF, et al. (2006) Selective fluorescent imaging of superoxide in vivo using ethidium-based probes. Proc Natl Acad Sci U S A 103: 15038–15043.

39. Chiba Y, Yamashita Y, Ueno M, Fujisawa H, Hirayoshi K, et al. (2005) Cultured murine dermal fibroblast-like cells from senescence-accelerated mice as in vitro models for higher oxidative stress due to mitochondrial alterations. J Gerontol A Biol Sci Med Sci 60: 1087–1098.
40. Drukarch B, van Muiswinkel FL (2001) Neuroprotection for Parkinson's disease: A new approach for a new millennium. Expert Opin Investig Drugs 10: 1855–1868.
41. Wu DC, Teismann P, Tieu K, Vila M, Jackson-Lewis V, et al. (2003) NADPH oxidase mediates oxidative stress in the 1-methyl-4-phenyl-1,2,3,6-tetrahydropyridine model of Parkinson's disease. Proc Natl Acad Sci U S A 100: 6145–6150.
42. Petroske E, Meredith GE, Callen S, Totterdell S, Lau YS (2001) Mouse model of Parkinsonism: a comparison between subacute MPTP and chronic MPTP/probenecid treatment. Neuroscience 106: 589–601.
43. Mitsumoto Y, Watanabe A, Mori A, Koga N (1998) Spontaneous regeneration of nigrostriatal dopaminergic neurons in MPTP-treated C57BL/6 mice. Biochem Biophys Res Commun 248: 660–663.
44. Song DD, Haber SN (2000) Striatal responses to partial dopaminergic lesion: evidence for compensatory sprouting. J Neurosci 20: 5102–5114.
45. Du X, Stull ND, Iacovitti L (1995) Brain-derived neurotrophic factor works coordinately with partner molecules to initiate tyrosine hydroxylase expression in striatal neurons. Brain Res 680: 229–233.
46. Betarbet R, Turner R, Chockkan V, DeLong MR, Allers KA, et al. (1997) Dopaminergic neurons intrinsic to the primate striatum. J Neurosci 17: 6761–6768.
47. Meredith GE, Farrell T, Kellaghan P, Tan Y, Zahm DS, et al. (1999) Immunocytochemical characterization of catecholaminergic neurons in the rat striatum following dopamine-depleting lesions. Eur J Neurosci 11: 3585–3596.
48. Grima B, Lamouroux A, Boni C, Julien JF, Javoy-Agid F, et al. (1987) A single human gene encoding multiple tyrosine hydroxylases with different predicted functional characteristics. Nature 326: 707–711.
49. Greenamyre JT, Hastings TG (2004) Biomedicine. Parkinson's–divergent causes, convergent mechanisms. Science 304: 1120–1122.
50. Betarbet R, Sherer TB, MacKenzie G, Garcia-Osuna M, Panov AV, et al. (2000) Chronic systemic pesticide exposure reproduces features of Parkinson's disease. Nat Neurosci 3: 1301–1306.
51. Höglinger GU, Carrard G, Michel PP, Medja F, Lombès A, et al. (2003) Dysfunction of mitochondrial complex I and the proteasome: interactions between two biochemical deficits in a cellular model of Parkinson's disease. J Neurochem 86: 1297–1307.
52. Rommelfanger KS, Edwards GL, Freeman KG, Liles LC, Miller GW, et al. (2007) Norepinephrine loss produces more profound motor deficits than MPTP treatment in mice. Proc Natl Acad Sci USA 104: 13804–13809.
53. Ohashi S, Mori A, Kurihara N, Mitsumoto Y, Nakai M (2006) Age-related severity of dopaminergic neurodegeneration to MPTP neurotoxicity causes motor dysfunction in C57BL/6 mice. Neurosci Lett 401: 183–187.
54. Shigenaga MK, Hagen TM, Ames BN (1994) Oxidative damage and mitochondrial decay in aging. Proc Natl Acad Sci USA 91: 10771–10778.
55. Iida T, Furuta A, Kawashima M, Nishida J, Nakabeppu Y, et al. (2001) Accumulation of 8-oxo-2′-deoxyguanosine and increased expression of hMTH1 protein in brain tumors. Neuro-oncol 3: 73–81.
56. Shimura-Miura H, Hattori N, Kang D, Miyako K, Nakabeppu Y, et al. (1999) Increased 8-oxo-dGTPase in the mitochondria of substantia nigral neurons in Parkinson's disease. Ann Neurol 46: 920–924.
57. Nunomura A, Perry G, Aliev G, Hirai K, Takeda A, et al. (2001) Oxidative damage is the earliest event in Alzheimer disease. J Neuropathol Exp Neurol 60: 759–767.
58. Kikuchi H, Furuta A, Nishioka K, Suzuki SO, Nakabeppu Y, et al. (2002) Impairment of mitochondrial DNA repair enzymes against accumulation of 8-oxo-guanine in the spinal motor neurons of amyotrophic lateral sclerosis. Acta Neuropathol 103: 408–414.
59. Tsuzuki T, Egashira A, Igarashi H, Iwakuma T, Nakatsuru Y, et al. (2001) Spontaneous tumorigenesis in mice defective in the MTH1 gene encoding 8-oxo-dGTPase. Proc Natl Acad Sci U S A 98: 11456–11461.
60. Sakamoto K, Tominaga Y, Yamauchi K, Nakatsu Y, Sakumi K, et al. (2007) MUTYH-null mice are susceptible to spontaneous and oxidative-stress-induced intestinal tumorigenesis. Cancer Res 67: 6599–6604.
61. Sakumi K, Tominaga Y, Furuichi M, Xu P, Tsuzuki T, et al. (2003) Ogg1 knockout-associated lung tumorigenesis and its suppression by Mth1 gene disruption. Cancer Res 63: 902–905.
62. Franklin KB, Paxinos G (2001) The Mouse Brain in Stereotaxic Coordinates (New York: Academic Press).
63. Kajitani K, Nomaru H, Ifuku M, Yutsudo N, Dan Y, et al. (2009) Galectin-1 promotes basal and kainate-induced proliferation of neural progenitors in the dentate gyrus of adult mouse hippocampus. Cell Death Differ 16: 417–27.
64. Mallajosyula JK, Kaur D, Chinta SJ, Rajagopalan S, Rane A, et al. (2008) MAO-B elevation in mouse brain astrocytes results in Parkinson's pathology. PLoS One 3: e1616.
65. Mount MP, Lira A, Grimes D, Smith PD, Faucher S, et al. (2007) Involvement of interferon-gamma in microglial-mediated loss of dopaminergic neurons. J Neurosci 27: 3328–37.
66. West MJ, Slomianka L, Gundersen HJ (1991) Unbiased stereological estimation of the total number of neurons in the subdivisions of the rat hippocampus using the optical fractionator. Anat Rec 231: 482–497.
67. Crabbe JC, Rigter H, Kerbusch S (1982) Analysis of behavioural responses to an ACTH analog in CXB/By recombinant inbred mice. Behav Brain Res 4: 289–314.
68. Przedborski S, Jackson-Lewis V, Yokoyama R, Shibata T, Dawson VL, et al. (1996) Role of neuronal nitric oxide in MPTP (1-methyl-4-phenyl-1,2,3,6-tetrahydropyridine)-induced dopaminergic neurotoxicity. Proc Natl Acad Sci USA 93: 4565–4571.
69. Liberatore GT, Jackson-Lewis V, Vukosavic S, Mandir AS, Vila M, et al. (1999) Inducible nitric oxide synthase stimulates dopaminergic neurodegeneration in the MPTP model of Parkinson disease. Nat Med 5: 1403–1409.

nature genetics

A genome-wide association study identifies three new susceptibility loci for ulcerative colitis in the Japanese population

Kouichi Asano[1–3], Tomonaga Matsushita[1,2], Junji Umeno[1,2], Naoya Hosono[1], Atsushi Takahashi[4], Takahisa Kawaguchi[5], Takayuki Matsumoto[2], Toshiyuki Matsui[6], Yoichi Kakuta[7], Yoshitaka Kinouchi[7], Tooru Shimosegawa[7], Masayo Hosokawa[8], Yoshiaki Arimura[8], Yasuhisa Shinomura[8], Yutaka Kiyohara[3], Tatsuhiko Tsunoda[5], Naoyuki Kamatani[4], Mitsuo Iida[2], Yusuke Nakamura[9] & Michiaki Kubo[1–3]

Ulcerative colitis is one of the principal forms of inflammatory bowel disease with complex manifestations. Although previous studies have indicated that there is a genetic contribution to the pathogenesis of ulcerative colitis, the genes influencing susceptibility to the disease have not been fully determined. To identify genetic factors conferring risk of ulcerative colitis, here we conducted a two-stage genome-wide association study and subsequent replication study using 1,384 Japanese individuals with ulcerative colitis and 3,057 control subjects. In addition to the expected strong association with the major histocompatibility complex (MHC) region, we identified three new susceptibility loci: the immunoglobulin receptor gene *FCGR2A* (rs1801274, $P = 1.56 \times 10^{-12}$), a locus on chromosome 13q12 (rs17085007, $P = 6.64 \times 10^{-8}$) and the glycoprotein gene *SLC26A3* (rs2108225, $P = 9.50 \times 10^{-8}$). rs1801274 is a nonsynonymous SNP of *FCGR2A* that is reported to have a critical effect on receptor binding affinity for IgG and to be associated with other autoimmune diseases. Our findings provide insight into the molecular pathogenesis of ulcerative colitis.

Ulcerative colitis is a major phenotype of inflammatory bowel disease (IBD) that is characterized by repeated chronic inflammation of the gastrointestinal tract[1]. Although the incidence and prevalence of ulcerative colitis have reached a plateau in northern Europe and North America, they continue to rise in southern Europe and Asia[2].

Twin studies have indicated that genetic factors are involved in the development of ulcerative colitis[3]. Although genome-wide association studies (GWAS) have identified many genes linked to susceptibility for Crohn's disease[4–8], there have been few GWAS of ulcerative colitis[9,10]. In studies examining whether loci linked to Crohn's disease susceptibility are also associated with ulcerative colitis, only a few loci have been shown to be associated with both diseases[9,11,12]. In addition, there are population differences in Crohn's disease susceptibility loci. For example, *CARD15* (also called *NOD2*), *IL23R* and *ATG16L1* are consistently implicated in European and North American populations, but have shown no association in Japanese populations[13,14]. Although an aberrant response of the intestinal immune system is important in the pathogenesis of IBD, typical features of Crohn's disease and ulcerative colitis differ with respect to disease localization and endoscopic and histological findings[1]. These results suggest that

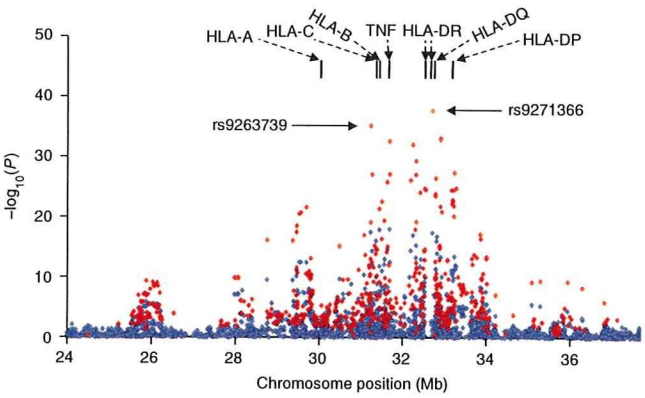

Figure 1 Results for association of the extended MHC region (Chr. 6, 24–38 Mb) with ulcerative colitis. Values of $-\log_{10}(P)$ are plotted against chromosome position, which is based on NCBI Build 36 coordinates. Blue diamonds represent Cochran-Armitage *P* values in the first set; red diamonds represent Cochran-Armitage *P* values in the combined analysis of the first and second sets. All *P* values were corrected by the method of genomic control.

[1]Laboratory for Genotyping Development, Center for Genomic Medicine, RIKEN, Yokohama Institute, Yokohama, Japan. [2]Department of Medicine and Clinical Science and [3]Department of Environmental Medicine, Graduate School of Medical Sciences, Kyushu University, Fukuoka, Japan. [4]Laboratory for Statistical Analysis and [5]Laboratory for Medical Informatics, Center for Genomic Medicine, RIKEN, Yokohama Institute, Japan. [6]Department of Gastroenterology, Fukuoka University Chikushi Hospital, Fukuoka, Japan. [7]Division of Gastroenterology, Tohoku University Graduate School of Medicine, Sendai, Japan. [8]First Department of Internal Medicine, Sapporo Medical University School of Medicine, Sapporo, Japan. [9]Laboratory of Molecular Medicine, Human Genome Center, Institute of Medical Science, University of Tokyo, Tokyo, Japan. Correspondence should be addressed to M.K. (mkubo@src.riken.jp).

Received 3 March; accepted 25 August; published online 15 November 2009; doi:10.1038/ng.482

Table 1 Summary of the GWAS and replication study results

SNP	Minor allele	Chr. location	Gene(s) or locus	Study	No. of samples		MAF		*P* value	OR	95% CI
					Case	Ctrl	Case	Ctrl			
rs9263739	T	6: 31,219,335	HLA	First set	373	934	0.295	0.143	3.07×10^{-18}	2.51	(2.05–3.08)
				Second set	376	1,097	0.310	0.153	2.83×10^{-19}	2.51	(2.07–3.05)
				Combined GWAS	749	2,031			6.95×10^{-36}	2.51	(2.17–2.90)
				Replication set 1	259	650	0.284	0.114	1.58×10^{-18}	3.18	(2.42–4.18)
				Replication set 2	376	376	0.273	0.104	7.25×10^{-17}	3.23	(2.43–4.29)
				Combined rep	635	1,026			9.17×10^{-34}	3.15	(2.61–3.79)
				Combined all	1,384	3,057			4.15×10^{-67}	2.73	(2.43–3.07)
rs1801274	G	1: 159,746,369	*FCGR2A*	First set	373	934	0.157	0.214	1.55×10^{-3}	0.68	(0.54–0.85)
				Second set	376	1,091	0.144	0.216	6.86×10^{-5}	0.61	(0.49–0.77)
				Combined GWAS	749	2,025			4.62×10^{-7}	0.65	(0.54–0.77)
				Replication set 1	259	649	0.162	0.206	3.39×10^{-2}	0.75	(0.57–0.98)
				Replication set 2	372	374	0.134	0.231	1.05×10^{-6}	0.52	(0.39–0.68)
				Combined rep	631	1,023			6.87×10^{-7}	0.62	(0.51–0.75)
				Combined all	1,380	3,048			1.56×10^{-12}	0.63	(0.55–0.72)
rs17085007	C	13: 26,429,267	No gene	First set	373	933	0.284	0.208	8.15×10^{-5}	1.51	(1.24–1.84)
				Second set	375	1,095	0.269	0.226	2.86×10^{-2}	1.26	(1.04–1.51)
				Combined GWAS	748	2,028			1.46×10^{-5}	1.38	(1.19–1.60)
				Replication set 1	258	649	0.285	0.226	7.21×10^{-3}	1.38	(1.09–1.75)
				Replication set 2	375	375	0.275	0.231	5.98×10^{-2}	1.26	(1.00–1.60)
				Combined rep	633	1,024			1.16×10^{-3}	1.32	(1.11–1.56)
				Combined all	1,381	3,052			6.64×10^{-8}	1.35	(1.21–1.51)
rs2108225	A	7: 107,240,339	*SLC26A3*	First set	373	933	0.288	0.363	6.09×10^{-4}	0.71	(0.59–0.86)
				Second set	376	1,096	0.306	0.354	2.42×10^{-2}	0.80	(0.67–0.96)
				Combined GWAS	749	2,029			6.16×10^{-5}	0.76	(0.65–0.87)
				Replication set 1	259	650	0.301	0.358	2.34×10^{-2}	0.78	(0.63–0.97)
				Replication set 2	375	375	0.300	0.365	6.73×10^{-3}	0.74	(0.60–0.92)
				Combined rep	634	1,025			4.24×10^{-4}	0.76	(0.65–0.89)
				Combined all	1,383	3,054			9.50×10^{-8}	0.76	(0.68–0.84)
rs10975003	C	9: 5,203,687	*JAK2, INSL6, INSL4*	First set	373	934	0.217	0.175	1.84×10^{-2}	1.31	(1.06–1.61)
				Second set	376	1,094	0.254	0.192	8.24×10^{-4}	1.43	(1.17–1.73)
				Combined GWAS	749	2,028			5.05×10^{-5}	1.38	(1.17–1.61)
				Replication set 1	259	647	0.230	0.182	2.42×10^{-2}	1.32	(1.04–1.69)
				Replication set 2	373	376	0.227	0.191	9.70×10^{-2}	1.24	(0.96–1.59)
				Combined rep	632	1,023			5.68×10^{-3}	1.29	(1.07–1.54)
				Combined all	1,381	3,051			1.09×10^{-6}	1.34	(1.18–1.51)

some genetic factors may be common between ulcerative colitis and Crohn's disease, whereas others are specific to either ulcerative colitis or Crohn's disease. In addition, ulcerative colitis susceptibility loci may also differ between European and Japanese people.

To identify genetic factors influencing ulcerative colitis susceptibility in the Japanese population, we performed a two-stage GWAS of 752 individuals with ulcerative colitis and 2,062 control subjects. In the first stage, 561,466 SNPs were genotyped for 376 individuals with ulcerative colitis (cases), and their allele frequencies were compared with those of 934 unaffected controls. Of these SNPs, we selected the top 12,000 SNPs and further genotyped them in independent samples. After the quality control process, the genotypes of 9,665 SNPs in an additional 376 cases and 1,097 controls were obtained in the second stage of the GWAS. Principal component analysis (PCA) showed no evidence of genetic heterogeneity in either the first or second set; however, the genomic control inflation factor (λ_{GC}) was 1.118 in the first set and 1.148 in the second set, suggesting the possibility of genotype misclassification or the existence of a population substructure. We applied stringent quality control criteria in each step, and the concordance rates among genotypes in the different platforms were extremely high; therefore, we considered that genotype misclassification might not be the cause of the difference in λ_{GC}. Because we have previously reported the existence of a population substructure in the Japanese population[15], we performed PCA using only the Japanese in Tokyo, Japan (JPT) and Han Chinese in Beijing, China (CHB) HapMap samples as references. However, this analysis revealed no clear population substructure (**Supplementary Fig. 1**). We therefore used λ_{GC}-corrected *P* values (P_{GC}) to adjust for the unknown genetic heterogeneity of the GWAS results[16].

We found that the major histocompatibility (MHC) region had a strong effect on ulcerative colitis susceptibility in the Japanese population as compared with European populations[9,10]. Combined analysis using the first and second sets identified 231 SNPs with highly significant association ($P_{GC} < 5 \times 10^{-7}$) located from 25.8 to 36.3 Mb on chromosome 6 (**Fig. 1**). Among these broad and strong associations, a peak of association was located between *HLA-DRB1* and *HLA-DQA1* (rs9271366; $P_{GC} = 2.13 \times 10^{-38}$). A second peak lay close to *HLA-B* (rs9263739; $P_{GC} = 6.95 \times 10^{-36}$). We speculate that these results might reflect the reported association of the HLA-DRB1*1502 or HLA-B*52 allele with ulcerative colitis in Japanese individuals[17]. Because we did

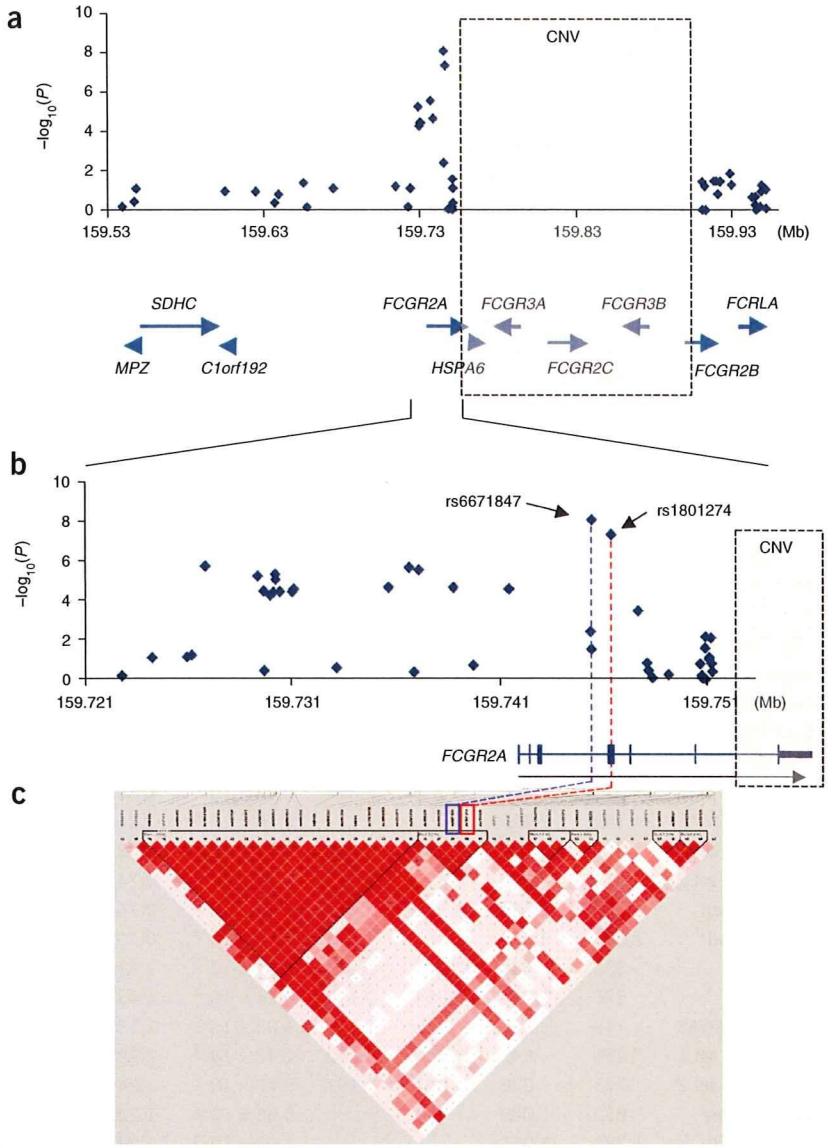

Figure 2 Association mapping and LD structure of the ulcerative colitis–associated region around *FCGR2A*. (**a**) Fine mapping using screening samples. Arrows indicate the positions of known genes. We could not genotype SNPs in the region of copy number variation (CNV) (see main text). (**b**) Resequencing using screening samples. (**c**) LD structure of the ulcerative colitis critical region. Shown are *D′* estimates for 44 common SNPs in cases and controls, where increasing shades of red indicate higher *D′* values.

not genotype HLA alleles, we could not clarify the linkage disequilibrium (LD) relationship between these HLA alleles and the associated SNPs. Because of the complex LD pattern in this region, however, it was difficult to determine precisely where the susceptibility genes are located. In addition, it is possible that the presence of a strong MHC association might obscure association signals elsewhere. Comprehensive experiments will be required to clarify these issues.

To identify susceptibility loci outside the MHC region, we selected the top 15 SNPs after considering LD (**Supplementary Table 1**) and genotyped them using two independent sets. After excluding two SNPs with a call rate of < 0.98, we analyzed 13 SNPs and replicated four loci (**Table 1** and **Supplementary Table 2**). Among them, rs1801274, rs17085007 and rs2108225 showed a significant level of replication even after Bonferroni correction ($P < 0.0038$).

The most significant association was observed at rs1801274, a nonsynonymous SNP (H131R) of *FCGR2A* ($P_{GC} = 1.56 \times 10^{-12}$, odds ratio (OR) = 0.63, 95% confidence interval (c.i.) = 0.55–0.72). This nonsynonymous SNP is considered to be important in the elimination of immune complexes[18]. The affinity of the Arg131 variant of FcγRIIa for all human IgG subclasses is lower than that of the His131 variant[18]. The Arg131 variant of FcγRIIa has also been reported to be functionally causative in systemic lupus erythematosus (SLE)[19,20], Guillain-Barré syndrome[18], multiple sclerosis[18] and type 1 diabetes[21]. Our study showed, however, that the His131 variant is the susceptibility allele for ulcerative colitis, a reversal of the genetic effect observed in other autoimmune diseases. According to the NCBI database, the His131 variant of FcγRIIa is conserved in *Pan troglodytes* and *Mus musculus*, but not in *Rattus norvegicus*. The susceptibility allele frequency differs among populations (0.491 in the CEPH Utah residents with ancestry from northern and western Europe sample (CEU); 0.496 in the HapMap Yoruba in Ibadan, Nigeria (YRI) sample; 0.685 in CHB; and 0.831 in JPT).

To define further SNPs associated with the disease, we performed fine mapping of the region including the *FCGR2A* gene using 51 tag SNPs (**Fig. 2a** and **Supplementary Table 3**). Of the 50 SNPs successfully genotyped, rs6671847 located at intron 3 showed the strongest association with ulcerative colitis ($P = 8.50 \times 10^{-9}$). LD analysis showed that rs1801274 represents a block of LD spanning from upstream of the 5′ UTR to intron 5 of *FCGR2A*. We resequenced a 27-kb region including this LD block using 94 individuals with ulcerative colitis and detected 29 new SNPs in addition to 62 known SNPs. We additionally genotyped 44 SNPs with a minor allele frequency of ≥ 0.05, but no SNP showed a stronger association than rs1801274 (**Fig. 2b**). Haplotype analysis indicated that a two-marker haplotype (rs1801274-rs6671847) had a similar degree of association with ulcerative colitis ($P = 9.37 \times 10^{-9}$). Logistic regression analysis demonstrated a weak association signal of rs6671847 after adjustment for rs1801274 ($P = 0.035$). Because rs1801274 is known as the functional variant affecting immune response[18], we considered that rs1801274 is probably the true causative variant and that rs6671847 might have an additional effect on ulcerative colitis susceptibility. However, functional analysis will be needed to clarify this issue.

During fine mapping, we identified a copy number variant (CNV) lying close to rs1801274. This CNV spans a 160-kb region and includes FCGR gene family members (**Fig. 2**). We therefore developed four TaqMan assays covering the whole *FCGR2A* gene (**Supplementary Fig. 2**) and found that the CNV was located in a region downstream of intron 6 of *FCGR2A* that did not include rs1801274. In addition, we

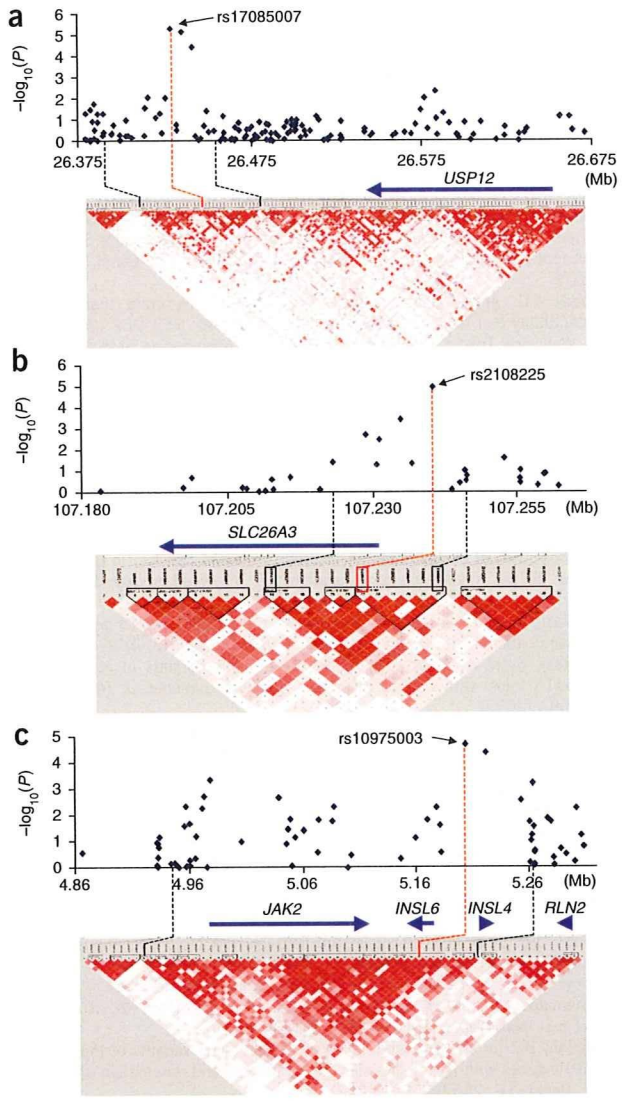

Figure 3 Fine mapping of ulcerative colitis–associated regions across 13q12.13, 7q31.1 and 9p24.1 using screening samples. (**a**) Chromosome 13q12.13. (**b**) *SLC26A3*. (**c**) The *JAK2-INSL6-INSL4* locus. Top, values of $-\log_{10}$ Cochran-Armitage *P* are plotted against chromosome position. Bottom, LD analyses (*D′*) using SNPs with a minor allele frequency of >0.05 are shown by Haploview.

found no association of *FCGR2A* copy number with either rs1801274 or susceptibility to ulcerative colitis ($P = 0.29$; **Supplementary Table 4**). Among the FCGR genes in this CNV region, copy numbers of both the F158V variant of *FCGR3A* (rs396991) and *FCGR3B* have been associated with several immune diseases[21,22]. However, rs396991 showed no association with ulcerative colitis among individuals with two copies of *FCGR3A* ($P = 0.19$). *FCGR3B* copy number showed a weak association with ulcerative colitis ($P = 0.001$), but this association was not significant ($P = 0.08$) after adjustment for rs1801274.

We mapped a second locus (rs17085007) on chromosome 13q12.13. Fine mapping of a 290-kb region revealed that the associated region is 74 kb and contains no known genes (**Fig. 3a** and **Supplementary Table 3**). The gene nearest to this region is *USP12* (encoding ubiquitin-specific peptidase-12), but SNPs within or around *USP12* showed no association with ulcerative colitis. We propose that this region might contain regulatory sequences or might express a transcript that is not yet identified.

We mapped a third locus (rs2108225) 9.5 kb upstream of *SLC26A3*. Fine mapping revealed that rs2108225 had the strongest association with ulcerative colitis, and the associated region was located in *SLC26A3* (**Fig. 3b**). Haplotype analyses of five SNPs (rs17154444, rs7810937, rs7785539, rs2108225 and rs6951457) in this block of LD revealed that a haplotype (TAGGA) showed a stronger association than rs2108225 ($P = 4.58 \times 10^{-6}$). Because resequencing the exons of *SLC26A3* revealed no associated SNPs, we suggest that functional variants that alter *SLC26A3* transcriptional activity might exist in this haplotype.

A fourth locus (rs10975003) included three genes in the same block of LD (**Fig. 3c**). This block included a previously identified locus for susceptibility to ulcerative colitis[9] (rs10974944; $D' = 0.92$ to rs10975003) and Crohn's disease[7] (rs10758669; $D' = 0.70$ to rs10975003), indicating that this region is a shared genetic risk locus for IBD.

We also evaluated the association of SNPs previously identified from European GWAS[9,10] (**Supplementary Table 5**). SNPs in the MHC region showed a strong association with ulcerative colitis in our Japanese subjects, but this association was weaker than the other associations identified in this study. We also replicated the association of chromosome 1p36 and *JAK2* with ulcerative colitis, but other loci showed no association. Some SNPs in *IL10* and *IL23R* were not polymorphic in our Japanese samples.

We also tested the association of the four SNPs identified in this study with subphenotypes of ulcerative colitis. When the cases were stratified by age of onset or disease extension, the four SNPs were associated similarly with every subphenotype (**Supplementary Table 6**). We could not estimate the effects of a history of colectomy or smoking habit at onset due to the small number of cases of each subphenotype.

Our GWAS identified a strong association between ulcerative colitis and SNPs in *FCGR2A*, which encodes an activating-type Fcγ receptor (FcγRIIa). FcγRIIa is expressed on the surface of several immune cells and binds immunoglobulins to induce various functions[18]. Accumulating evidence suggests that an aberrant response to intestinal microbes has a crucial role in the pathogenesis of ulcerative colitis[1]. High populations of mucosal B cells and plasma cells, which are associated with increases in autoantibodies, are frequently found in ulcerative colitis[23]. Engagement of FcγRIIa with IgG antibodies is reported[24] to induce secretion of tumor necrosis factor-α. In addition, abnormal IgG function in response to pathogens can trigger aberrant immune manifestations. Our findings indicate that antibody-mediated adaptive immunity mediated through FcγRIIa may have a pivotal role in, and account for part of the mechanism of, the type 2 T-helper cell–polarized immune response in ulcerative colitis.

FCGR2A is reported to be a susceptibility gene for other autoimmune diseases, and the H131R substitution in FcγRIIa is considered to have functional significance. His131 is located at the IgG-binding site of FcγRIIa[18]. The H131R amino acid change affects the receptor's recognition of immunoglobulins[25] and increases its binding affinity for immune complexes, resulting in an increase in both the phagocytic capacity of polymorphonuclear leukocytes and cytokine production. In SLE, individuals with the Arg131 variant of FcγRIIa have weaker binding affinity for human IgG and are thought to have a lower capacity for immune complex elimination, which might lead to the glomerular immune complex deposition observed in lupus nephritis[19]. By contrast, a higher capacity for immune complex handling in subjects with the His131 variant would lead to hyperactivation of immune cells. Such hyperactivation could induce

a higher capacity for antigen presentation to T cells and activation of B cells, as well as the overproduction of cytokines. We therefore speculate that individuals with the His131 variant of FcγRIIa may experience the hyperactivation of multiple immune cells, resulting in perpetual inflammation of the colorectal mucosa after immune complex production from some antigens. Our findings imply that the immune complex pathway mediated through FcγRIIa is important in the etiology of ulcerative colitis.

The SLC26A3 protein is a transmembrane glycoprotein that is reported to be localized in the mucosal epithelium of the lower intestinal tract and is known to function mainly as a sulfate transporter that reabsorbs Cl^- ions into the epithelium and excretes HCO_3^- into the intestinal lumen[26]. Mutations in *SLC26A3* have been reported to cause congenital chloride diarrhea[27]. Expression of the glycoprotein is reduced in the surface epithelium of individuals with ulcerative colitis and in animal models of spontaneous colitis[28]. In addition, enteropathogenic *Escherichia coli* infection reduces intestinal Cl^-–OH^- exchange activity after decreasing *SLC26A3* transcripts[29]. These results suggest that ulcerative colitis susceptibility alleles in *SLC26A3* may act as a silencer, and the reduction in transcripts might contribute to ulcerative colitis susceptibility.

In summary, our GWAS identified three new ulcerative colitis susceptibility loci by using 1,384 cases and 3,057 controls. Our findings should shed light on the pathogenesis of ulcerative colitis and other autoimmune diseases.

METHODS

Methods and any associated references are available in the online version of the paper at http://www.nature.com/naturegenetics/.

Accession codes. JSNP: genotype data of the 934 controls in the first set, JSNP550typed.

Note: Supplementary information is available on the Nature Genetics website.

ACKNOWLEDGMENTS

We thank all of the patients who participated in this study. We are grateful to F. Hirai, K. Aoyagi, T. Fuchigami, M. Miyazaki, S. Yada, M. Esaki, H. Koga, S. Nakamura, S. Motoya, M. Nomura and T. Sonoda for collecting samples. We thank R. Nakamichi and T. Morizono for help with statistical analysis; participants of the Midosuji and other related Rotary Clubs, Hisayama residents and staff of the Division of Health and Welfare of Hisayama for cooperation in this study; and K. Ashikawa, H. Amitani and other staff of the Laboratory for Genotyping Development, Center for Genomic Medicine, for contributions to this study. This work was supported in part by the Ministry of Education, Culture, Sports, Science and Technology.

AUTHOR CONTRIBUTIONS

Y.N., N.K., M.K. and K.A. designed the study. K.A., T. Matsushita and N.H. performed the genotyping. A.T., T.K., T.T. and N.K. performed the data analyses. J.U., T. Matsumoto, T. Matsui and Y. Kiyohara managed the DNA samples and clinical information of the GWAS. Y. Kakuta, Y. Kinouchi and T.S. performed the genotyping in the first replication study. M.H., Y.A. and Y.S. performed the genotyping in the second replication study. Y.N., M.K., J.U. and K.A. wrote the manuscript. M.I., Y.N. and M.K. supervised the study.

Published online at http://www.nature.com/naturegenetics/.
Reprints and permissions information is available online at http://npg.nature.com/reprintsandpermissions/.

1. Podolsky, D.K. Inflammatory bowel disease. *N. Engl. J. Med.* **347**, 417–429 (2002).
2. Loftus, E.V. Jr. Clinical epidemiology of inflammatory bowel disease: Incidence, prevalence, and environmental influences. *Gastroenterology* **126**, 1504–1517 (2004).
3. Halme, L. *et al.* Family and twin studies in inflammatory bowel disease. *World J. Gastroenterol.* **12**, 3668–3672 (2006).
4. Yamazaki, K. *et al.* Single nucleotide polymorphisms in *TNFSF15* confer susceptibility to Crohn's disease. *Hum. Mol. Genet.* **14**, 3499–3506 (2005).
5. Duerr, R.H. *et al.* A genome-wide association study identifies *IL23R* as an inflammatory bowel disease gene. *Science* **314**, 1461–1463 (2006).
6. Hampe, J. *et al.* A genome-wide association scan of nonsynonymous SNPs identifies a susceptibility variant for Crohn disease in *ATG16L1*. *Nat. Genet.* **39**, 207–211 (2007).
7. Barrett, J.C. *et al.* Genome-wide association defines more than 30 distinct susceptibility loci for Crohn's disease. *Nat. Genet.* **40**, 955–962 (2008).
8. The Wellcome Trust Case Control Consortium. Genome-wide association study of 14,000 cases of seven common diseases and 3,000 shared controls. *Nature* **447**, 661–678 (2007).
9. Franke, A. *et al.* Sequence variants in *IL10, ARPC2* and multiple other loci contribute to ulcerative colitis susceptibility. *Nat. Genet.* **40**, 1319–1323 (2008).
10. Silverberg, M.S. *et al.* Ulcerative colitis-risk loci on chromosomes 1p36 and 12q15 found by genome-wide association study. *Nat. Genet.* **41**, 216–220 (2009).
11. Franke, A. *et al.* Replication of signals from recent studies of Crohn's disease identifies previously unknown disease loci for ulcerative colitis. *Nat. Genet.* **40**, 713–715 (2008).
12. Anderson, C.A. *et al.* Investigation of Crohn's disease risk loci in ulcerative colitis further defines their molecular relationship. *Gastroenterology* **136**, 523–529 (2009).
13. Yamazaki, K. *et al.* Absence of mutation in the *NOD2/CARD15* gene among 483 Japanese patients with Crohn's disease. *J. Hum. Genet.* **47**, 469–472 (2002).
14. Yamazaki, K. *et al.* Association analysis of genetic variants in *IL23R, ATG16L1* and 5p13.1 loci with Crohn's disease in Japanese patients. *J. Hum. Genet.* **52**, 575–583 (2007).
15. Yamaguchi-Kabata, Y. *et al.* Japanese population structure, based on SNP genotypes from 7003 individuals compared to other ethnic groups: effects on population-based association studies. *Am. J. Hum. Genet.* **83**, 445–456 (2008).
16. Devlin, B. & Roeder, K. Genomic control for association studies. *Biometrics* **55**, 997–1004 (1999).
17. Futami, S. *et al.* HLA-DRB1*1502 allele, subtype of DR15, is associated with susceptibility to ulcerative colitis and its progression. *Dig. Dis. Sci.* **40**, 814–818 (1995).
18. Takai, T. Roles of Fc receptors in autoimmunity. *Nat. Rev. Immunol.* **2**, 580–592 (2002).
19. Salmon, J.E. *et al.* FcγRIIA alleles are heritable risk factors for lupus nephritis in African Americans. *J. Clin. Invest.* **97**, 1348–1354 (1996).
20. Harley, J.B. *et al.* Genome-wide association scan in women with systemic lupus erythematosus identifies susceptibility variants in *ITGAM, PXK, KIAA1542* and other loci. *Nat. Genet.* **40**, 204–210 (2008).
21. Alizadeh, B.Z. *et al.* Association analysis of functional variants of the FcγRIIa and FcγRIIIa genes with type 1 diabetes, celiac disease and rheumatoid arthritis. *Hum. Mol. Genet.* **16**, 2552–2559 (2007).
22. Fanciulli, M. *et al. FCGR3B* copy number variation is associated with susceptibility to systemic, but not organ-specific, autoimmunity. *Nat. Genet.* **39**, 721–723 (2007).
23. Farrell, R.J. & Peppercorn, M.A. Ulcerative colitis. *Lancet* **359**, 331–340 (2002).
24. Clavel, C. *et al.* Induction of macrophage secretion of tumor necrosis factor α through Fcγ receptor IIa engagement by rheumatoid arthritis-specific autoantibodies to citrullinated proteins complexed with fibrinogen. *Arthritis Rheum.* **58**, 678–688 (2008).
25. Lu, J. *et al.* Structural recognition and functional activation of FcγR by innate pentraxins. *Nature* **456**, 989–992 (2008).
26. Hoglund, P. *et al.* Mutations of the Down-regulated in adenoma (DRA) gene cause congenital chloride diarrhoea. *Nat. Genet.* **14**, 316–319 (1996).
27. Moseley, R.H. *et al.* Downregulated in adenoma gene encodes a chloride transporter defective in congenital chloride diarrhea. *Am. J. Physiol.* **276**, G185–G192 (1999).
28. Yang, H. *et al.* Intestinal inflammation reduces expression of DRA, a transporter responsible for congenital chloride diarrhea. *Am. J. Physiol.* **275**, G1445–G1453 (1998).
29. Gill, R.K. *et al.* Mechanism underlying inhibition of intestinal apical Cl/OH exchange following infection with enteropathogenic *E. coli*. *J. Clin. Invest.* **117**, 428–437 (2007).

ONLINE METHODS

Samples. We conducted a two-stage GWAS using independent case-control sets (**Supplementary Table 7**). Samples from individuals with ulcerative colitis were collected from Kyushu University and 25 affiliated hospitals: Kyushu University Hospital (n = 129), Fukuoka University Chikushi Hospital (n = 106), Fukuoka University Hospital (n = 85), Saiseikai Kumamoto Hospital (n = 11), Yamaguchi Red Cross Hospital (n = 20), Matsuyama Red Cross Hospital (n = 113), Fukuoka Red Cross Hospital (n = 16), Chihaya Hospital (n = 19), Kyushu Central Hospital (n = 6), Hakujuji Hospital (n = 12), Health Insurance Nogata Chuou Hospital (n = 19), Kokura Medical Center (n = 15), Japan Seamen's Relief Association Moji Hospital (n = 2), Shimonoseki City Central Hospital (n = 6), Kama Red Cross Hospital (n = 3), Sasebo Chuo Hospital (n = 45), Nippon Steel Yawata Memorial Hospital (n = 33), Kimura Hospital (n = 13), Saiseikai Yahata General Hospital (n = 12), Kyushu Dental College Hospital (n = 1), Hamanomachi Hospital (n = 48), Kamata Hospital (n = 1), Kamori Clinic (n = 3), Kaita Hospital (n = 2), Sakura Hospital (n = 1) and Osamura Clinic (n = 31). Consequently, 752 individuals with ulcerative colitis were recruited under the standardized diagnostic criteria and were randomly divided into two sets. We used 376 samples from individuals with ulcerative colitis for the first stage and 376 for the second stage. Age, sex and clinical parameters did not differ between these two sets (**Supplementary Table 8**). For the control subjects, we used 934 volunteers recruited at the Midosuji and other related Rotary Clubs for the first stage (mean age, 52 ± 15 years old). Controls for the second stage were selected from participants in the Hisayama health survey[30] conducted between 2002 and 2003, after excluding subjects with a history of ulcerative colitis (mean age, 57 ± 10 years). The age and sex of subjects, and the geographical location of the recruitment centers, are shown in **Supplementary Table 7** and **Supplementary Figure 3**, respectively.

For the replication study, 265 individuals with ulcerative colitis and 665 healthy volunteers were recruited at Tohoku University Hospital from May 1998 to January 2006 (replication set 1). Individuals with ulcerative colitis for replication set 2 were recruited at Sapporo Medical University Hospital and seven affiliated hospitals (n = 64), Sapporo Kosei General Hospital (n = 249) and Teine Keijinkai Hospital (n = 63). Healthy controls for replication set 2 (n = 376) were recruited at the Department of Public Health, Sapporo Medical University.

Diagnosis of ulcerative colitis in all subjects was made by expert gastroenterologists in accordance with clinical, radiological, endoscopic and histological features based on established uniform criteria[31]. Namely, diagnosis of ulcerative colitis requires (i) chronic or recurrent symptoms of bloody (and mucous) stool; (ii) macroscopic appearance by endoscopy or barium enema of continuous mucosal inflammation affecting the rectum in continuity with some or all of the colon; (iii) microscopic features on biopsy including the presence of widespread and diffuse mucosal distortion, diffuse transmucosal lymphocytic inflammation, cryptitis and crypt abscesses; and (iv) no suspicious findings of Crohn's disease, indeterminate colitis, infections, or other acute or chronic non-IBD conditions on small bowel radiograph, ileocolonoscopy, biopsy or stool examination. When endoscopic or histopathological findings of the individuals were divergent or inconclusive for diagnosis of ulcerative colitis or Crohn's disease, we regarded those subjects to have indeterminate colitis and excluded them from analysis. In terms of disease extent, proctitis was defined as inflammatory changes limited to the rectum. Left-sided colitis was defined as inflammatory changes up to the splenic flexure, and changes beyond the splenic flexure were defined as extensive colitis. Ulcerative proctitis is a milder ulcerative colitis subphenotype and is sometimes regarded as a separate phenotype because of its better prognosis. However, the clinical symptoms and histopathological findings of ulcerative proctitis are the same as those of other subphenotypes. In addition, the impact of the susceptibility loci identified in this study was not influenced by subphenotype. As a result, we included ulcerative proctitis in this study as a ulcerative colitis subphenotype.

The ethical committees of Kyushu University, Tohoku University, Sapporo Medical University and RIKEN approved this study, and written informed consent was obtained from all subjects.

Genotyping and data-quality filters. For the first-stage screening, 376 cases and 934 controls were genotyped by using an Illumina HumanHap550v3 Genotyping BeadChip. After excluding three cases with a call rate of < 0.98, we applied SNP quality control (call rate ≥ 0.99 in cases and controls, Hardy-Weinberg $P \geq 1 \times 10^{-6}$ in controls) and 513,923 autosomal SNPs that passed the quality filters were analyzed in the first stage. The genotype data of the 934 controls are available at the JSNP database. Of the SNPs analyzed in the first stage, we selected the top 12,000 SNPs with a minor allele frequency of ≥ 0.1 in either cases or controls after considering the statistical power required to detect associations for SNPs in the second stage. In the second stage, we genotyped an additional 376 ulcerative colitis cases and 1,128 controls by using an Affymetrix GeneChip Custom 10K array. After excluding 31 controls with a call rate of < 0.95, all cluster plots were checked by visual inspection by trained staff, and SNPs with an ambiguous call were excluded. As a result, 9,665 out of 10,635 SNPs assayed were analyzed in the second stage. We used a multiplex PCR-based Invader assay[32] for the replication study (including a replication study of previous GWAS) and fine mapping. Six cases and 15 controls were excluded from analysis owing to a low call rate in replication set 1. The concordance rate between genotypes determined by the Illumina HumanHap550v3 BeadChip and those determined by the Affymetrix GeneChip Custom 10K array among 94 duplicated samples was 0.9997. The concordance rate of 13 SNPs selected for the replication study was 0.999 between the Affymetrix GeneChip Custom 10K array and the multiplex PCR-based Invader assay. The reproducibility of the multiplex PCR-based Invader assay was 0.998 on the basis of duplicate assays of five SNPs among all samples analyzed.

Fine mapping and resequencing. We performed fine mapping for four ulcerative colitis–associated loci using all samples in the first and second sets. Haploview was used to select tag SNPs with a pairwise r^2 of > 0.90 and a minor allele frequency of ≥ 0.05 on the basis of HapMap JPT data. Resequencing of candidate regions was performed in 94 ulcerative colitis cases by using an ABI3730 Genetic Analyzer.

Estimation of gene copy numbers. To estimate gene copy number in the FCGR gene cluster, we conducted a quantitative real-time PCR assay (TaqMan assay, Applied Biosystems). We designed at least two probes that encompassed each gene by using Primer Express 1.5. These TaqMan probes were labeled with FAM dye at the 5′ end, linked by a nonfluorescence quencher, and tagged with MGB dye at the 3′ end. As a reference gene, we used the TaqMan Copy Number Reference Assay RNase P (Applied Biosystems). All TaqMan assays were performed by following reported protocols, and copy number calculation was conducted by the $\Delta\Delta Ct$ method[33]. We assumed that samples with a median ΔCt value were two-copy samples and used them as a calibrator. All samples were examined in quadruplicate, and the average copy number values were used in the scatter plot analysis. The primer and probe sequences of all assays are available from the authors on request. We calculated confidence in the predicted copy numbers, and samples with a prediction confidence of ≤ 0.95 were removed from further analyses (total call rate, 99.8%).

Statistics. For general statistical analysis, we used R statistical environment version 2.7.1 or PLINK. To draw the LD map, we used Haploview software. To select SNPs for the second stage, single-marker analysis in the first stage was carried out by allele frequency, dominant and recessive models using Fisher's exact test. The possible influence of population stratification was investigated by EIGENSTRAT software using all of the 442,793 autosomal SNPs located at the non-MHC region with a call rate of ≥ 0.99 and a minor allele frequency of ≥ 0.01. We also included genotypes obtained from four populations of the HapMap project for estimation of the population structure. For estimation of the population substructure, we included the genotypes of JPT and CHB of the Hapmap project only. To identify spurious associations resulting from more subtle stratification of the case and control populations, we also calculated the genomic control inflation measure[16] and plotted the observed distribution as compared with the expected distribution of P values (quantile-quantile plots). Single-marker analysis of each set was carried out by using the Cochran-Armitage trend test. P values for first and second set of the GWAS were corrected by the method of genomic control. Combined analysis of the data from different case-control sets was conducted by the inverse variance method using λ_{GC}-corrected P values in the first and second

set. Heterogeneities across the population were estimated formally by using Cochran's Q test. To test the association between ulcerative colitis and the copy number of genes in the FCGR locus, logistic regression analysis was used in all subjects for whom complete genotyping and copy number were available.

URLs. JSNP, http://snp.ims.u-tokyo.ac.jp/; R statistical environment, http://www.cran.r-project.org/; PLINK, http://pngu.mgh.harvard.edu/~purcell/plink/.

30. Kiyohara, Y. *et al.* Ten-year prognosis of stroke and risk factors for death in a Japanese community: the Hisayama study. *Stroke* **34**, 2343–2347 (2003).
31. Lennard-Jones, J.E. Classification of inflammatory bowel disease. *Scand. J. Gastroenterol. Suppl.* **170**, 2–6 (1989).
32. Ohnishi, Y. *et al.* A high-throughput SNP typing system for genome-wide association studies. *J. Hum. Genet.* **46**, 471–477 (2001).
33. Hosono, N. *et al.* Multiplex PCR-based real-time invader assay (mPCR-RETINA): a novel SNP-based method for detecting allelic asymmetries within copy number variation regions. *Hum. Mutat.* **29**, 182–189 (2008).

Clinical Chemistry 55:8
1546–1554 (2009)

CYP2D6 Genotyping for Functional-Gene Dosage Analysis by Allele Copy Number Detection

Naoya Hosono,[1*] Mamoru Kato,[2] Kazuma Kiyotani,[3] Taisei Mushiroda,[3] Sadaaki Takata,[1] Hiroko Sato,[1] Hanae Amitani,[1] Yumiko Tsuchiya,[1] Keiko Yamazaki,[1] Tatsuhiko Tsunoda,[2] Hitoshi Zembutsu,[4] Yusuke Nakamura,[1,4] and Michiaki Kubo[1]

BACKGROUND: Cytochrome P450 2D6 (CYP2D6), one of the most important drug-metabolizing enzymes, has been reported to possess variation in the encoding *CYP2D6* gene (cytochrome P450, family 2, subfamily D, polypeptide 6) that affects enzymatic activity. For the pharmacogenetic study of CYP2D6, accurate measurement of the dosage of the functional gene is essential; however, current genotyping techniques are insufficient because of their inability to provide the exact copy number of functional *CYP2D6* genes.

METHODS: We developed 3 quantitative real-time PCR (qPCR) assays for estimating the total copy number of the *CYP2D6* gene, as well as 24-multiplex PCR-based real-time Invader assays (mPCR-RETINAs) for estimating the allele ratio at each variation locus. After determining the allele copy number at each locus, we estimated the frequencies of *CYP2D6* alleles in a population and the diplotype in each individual by a CNVphaser (copy number variation phaser). The qPCR assays and RETINAs used for HapMap Japanese and Chinese samples were applied to 455 Japanese individuals.

RESULTS: Forty-two individuals (9.2%) had one *CYP2D6* gene copy, 207 (45.5%) had 2 copies, 161 (35.4%) had 3 copies, 40 (8.8%) had 4 copies, and 5 (1.1%) had 5 copies of the *CYP2D6* gene. We found 16 different *CYP2D6* alleles, with frequencies similar to those described in previous reports. In the diplotype analysis, we observed that *CYP2D6*1/*1* and **1/*10-*36* were the most common diplotypes (approximately 20%) in our population.

CONCLUSIONS: Our method is the first to determine the exact number of functional *CYP2D6* gene copies. We believe our method will facilitate and accelerate the detailed pharmacogenetic analysis of CYP2D6.

Cytochrome P450 2D6 (CYP2D6),[5] one of the key drug-metabolizing enzymes, is involved in the biotransformation of a large number of drugs, including β-blockers, antiarrhythmics, opioids, and a number of antidepressant and antipsychotic agents *(1)*. The *CYP2D6*[6] gene (cytochrome P450, family 2, subfamily D, polypeptide 6) is highly polymorphic, and >60 *CYP2D6* alleles have been reported (http://www.cypalleles.ki.se/). These *CYP2D6* alleles consist of combinations of variants of single-nucleotide polymorphisms, short insertions and deletions, gene conversions, and copy number variants or variations (CNVs), including deletion and duplications/multiplications of an entire gene. Approximately half of the reported *CYP2D6* alleles affect enzymatic activity in vivo or in vitro, and some of them are closely related to treatment failure or to the toxicity of drugs metabolized by CYP2D6 *(2–7)*.

We refer to the *CYP2D6* alleles (haplotypes of variants) summarized in the human *CYP* allele database as "*CYP2D6*-alleles," whereas we use the term "allele" only for each locus of variation. For example, *CYP2D6*10-*10* is defined as one *CYP2D6*-allele containing 2 copies of the *CYP2D6* gene with 100C>T alleles on one chromosome.

Several techniques have been reported for *CYP2D6* genotyping, including the combination of long PCR and RFLP *(8, 9)*, AmpliChip CYP450 (Roche) *(10, 11)*, and SNaPshot (Applied Biosystems) *(12)*; however, these methods detect only the presence or absence of each

[1] Laboratory for Genotyping Development, [2] Laboratory for Medical Informatics, and [3] Laboratory for Pharmacogenetics, Center for Genomic Medicine, RIKEN, Yokohama, Japan; [4] Laboratory of Molecular Medicine, Human Genome Center, The Institute of Medical Science, University of Tokyo, Tokyo, Japan.
* Address correspondence to this author at: 1-7-22 Suehiro-cho, Tsurumi, Yokohama, Kanagawa, 230-0045, Japan. Fax +81-45-503-9606; e-mail nhosono@src.riken.jp.
Received January 22, 2009; accepted May 26, 2009.
Previously published online at DOI: 10.1373/clinchem.2009.123620

[5] Nonstandard abbreviations: CYP2D6, cytochrome P450 2D6; CNV, copy number variant or variation; mPCR-RETINA, multiplex PCR–based real-time Invader assay; qPCR, quantitative PCR; JCH, Japanese and Chinese.
[6] Human genes: *CYP2D6*, cytochrome P450, family 2, subfamily D, polypeptide 6; *CYP2D7P1*, cytochrome P450, family 2, subfamily D, polypeptide 7 pseudogene 1.

CYP2D6-allele or variant. Because of their inability to provide the exact copy number of functional *CYP2D6* genes, these techniques are insufficient for estimating the functional effect of gene dosage on the efficacy or toxicity of drugs metabolized by CYP2D6 *(13, 14)*. In addition, these techniques require some improvements. Long PCR–RFLP, the gold standard for *CYP2D6* genotyping, has been reported to have a high rate of amplification failure (>40%) *(15)* and to cause false-positive/false-negative results in CNV detection because of unknown genomic alterations *(16, 17)*. Moreover, these techniques require multiple steps and long reaction times, leading to low throughputs.

Recently, we developed a multiplex PCR–based real-time Invader assay (mPCR-RETINA) that reveals the allele ratio at each locus within CNV regions by detecting allelic asymmetries *(18)*. By combining the allele ratio data with the data for total gene copy number obtained by real-time quantitative PCR (qPCR), we were able to measure the allele copy number at each locus *(18)*. We also developed CNVphaser software that can estimate both the haplotype frequency in a population and the diplotype of each individual within CNV regions *(19)*. We used these newly developed techniques to investigate how to determine the exact copy number of functional *CYP2D6* genes in each individual.

Materials and Methods

GENOMIC DNA

We used 90 HapMap Japanese and Chinese (JCH) samples for assay development. We excluded 2 samples (NA18996 and NA18540) reported to have cell line artifacts *(20)* and used 88 samples for the evaluation. All JCH samples were purchased from Coriell Cell Repositories. We tested the assays in samples from 455 anonymous Japanese individuals provided by Biobank Japan (http://www.biobankjp.org), which collected genomic DNA after the patients had provided written informed consent to participate in this project. This study was approved by the institutional review board of the Ethical Committee at RIKEN.

MEASUREMENT OF TOTAL GENE COPY NUMBER BY qPCR

To determine the total copy number, we developed hydrolysis probe assays (5′FL, Int2, and Int6) at 3 different sites within or around the *CYP2D6* gene (see Fig. 1 in the Data Supplement that accompanies the online version of this article at http://www.clinchem.org/content/vol55/issue8). Primers and probes were designed with the aid of Primer Express software v2.0 (Applied Biosystems) except for the reported assay of Int6 *(21)*. These hydrolysis probes were labeled with FAM at the 5′ end and linked at the 3′ end with a non-fluorescent quencher used in combination with a minor-groove binder moiety. Final concentrations of the primer and hydrolysis probe in 3 *CYP2D6* assays were 900 nmol/L and 200 nmol/L, respectively. As the reference gene, we used the commercially available TaqMan Copy Number Reference Assay RNase P (Applied Biosystems). All assays were performed with TaqMan Universal PCR Master Mix (Applied Biosystems) according to the recommended protocol. The hydrolysis probe reaction was performed in a 1-tube biplex assay on an ABI Prism 7900 instrument (Applied Biosystems). We performed all qPCR experiments with a 384-well format in a 10-μL reaction volume containing 10 ng genomic DNA. The qPCR thermal cycling conditions were as follows: initiation at 95 °C for 10 min for hot start, followed by 40 cycles of 95 °C for 15 s and 60 °C for 1 min.

Copy number was calculated by the $\Delta\Delta$Ct method, where Ct is the threshold cycle *(18, 21–23)*. The PCR efficiency of each assay was estimated from the calibration curves of a sample (NA18995) serially diluted from 40 ng to 2.5 ng of genomic DNA. PCR efficiency was calculated as $10^{-1/\text{slope}} - 1$ *(22, 23)*. We examined the calibration curves 4 times and calculated the mean PCR efficiency in each assay. Mean PCR efficiencies of all assays ranged from 0.96 to 0.99 (5′FL and RNase P, 0.977 and 0.988, respectively; Int2 and RNase P, 0.982 and 0.964, respectively; Int6 and RNase P, 0.962 and 0.975, respectively; see Fig. 2 in the online Data Supplement), and they fulfilled the reported criteria (0.9–1.1) for the $\Delta\Delta$Ct method *(23)*.

All samples were examined in quadruplicate, and the mean, SD, SE, CV, and 95% CI for the mean were calculated for each sample. Mean CV values were 4.57% for 5′FL, 2.35% for Int2, and 3.44% for Int6 in JCH samples and were 3.65%, 3.53%, and 4.65%, respectively, in the 455 Japanese samples. We analyzed mean copy number values and 95% CIs for each sample in scatter plots. When the 95% CIs of the mean copy number value (mean $\pm$ 1.96 $\times$ SE) overlapped each other, we estimated that these samples had the same copy number. Table 1 in the online Data Supplement lists the primer and probe sequences for all of the assays.

MEASUREMENT OF ALLELE RATIO BY RETINA

RETINA monitors the fluorescence intensity of each allele in real time during the Invader assay and detects allelic asymmetries caused by genomic duplication/multiplication in heterozygous individuals. Details for determining the allele ratio by RETINA have previously been described *(18)*. For the RETINA assay, we first amplified an entire *CYP2D6* gene region via a triplex PCR with the previously reported primers *(9, 15)*. We used Takara Ex *Taq* HS (Takara Bio) according to the manufacturer's instructions at a primer concentra-

tion of 250 nmol/L. Triplex PCR was performed on a GeneAmp 9700 PCR System (Applied Biosystems) in a 10-μL reaction volume containing 10 ng of genomic DNA. The PCR conditions were as follows: initiation at 95 °C for 2 min, 35 cycles of 98 °C for 10 s and 68 °C for 4 min, and termination at 68 °C for 7 min. We designed Invader assays according to the guideline recommended by Third Wave Technologies except for the reported 6 loci (100C>T, 883G>C, 1707delT, 1846G>A, 2549delA, and 2850C>T) *(15)*. Fluorescence resonance energy transfer probes labeled with FAM or Yakima Yellow were purchased from Third Wave Technologies. ROX dye (6-carboxy-X-rhodamine; Sigma–Aldrich) was used to normalize reporter signals. We carried out 24 RETINA assays in duplicate in a 4-μL reaction volume on an ABI Prism 7900 instrument with diluted triplex PCR products. The RETINA reaction conditions were 95 °C for 5 min followed by 63 °C for 10 min. The allele ratio at each locus was determined in each sample by analysis of allelic discrimination plots from calibration curves of the allele ratio (see Fig. 3 in the online Data Supplement) *(18)*.

CYP2D6 ALLELE ESTIMATION

We determined the allele copy number for each variant by combining the RETINA and qPCR results *(18)*. Allele copy number data were rounded to an integer *(18)* for haplotype/diplotype estimation of *CYP2D6* alleles by the CNVphaser *(19)*. We adopted estimated haplotypes satisfying the haplotype-frequency threshold of 0.001 (>1/2n) *(24)* and also referenced known *CYP2D6* alleles in the human CYP allele database. We defined *CYP2D6*1* as such when the estimated haplotype had the wild type at all tested loci. In diplotype analysis, we extracted the diplotypes with the highest diplotype probability score in each individual.

DIRECT SEQUENCING, LONG PCR, AND SOUTHERN-RFLP ANALYSIS

We performed direct sequencing to confirm the presence of variant alleles detected by RETINA with the ABI Prism 3700. Direct sequencing was performed with BigDye Terminator version 3.1 (Applied Biosystems) with the reported sequencing primers *(25)*. Sequence data were analyzed with SeqScape software (Applied Biosystems). We performed long PCR to confirm the estimated whole-gene deletion (*CYP2D6*5*) and duplications (*CYP2D6*1-*1*, **2–2*, **10-*10*, **10-*36*, and **36-*36*) according to the reported protocols *(16, 26)*. Furthermore, we performed Southern-RFLP analysis to confirm the new *CYP2D6* alleles (**10-*36-*36* and **10-*10-*36*) as previously described *(27)* by means of the AlkPhos Direct kit (GE Healthcare) for the Southern blot experiment.

Results

ASSAY DEVELOPMENT

We developed 3 qPCR assays with 88 JCH samples to determine the total copy number of the *CYP2D6* gene. Fig. 1 presents the mean total copy number and the 95% CI for each sample. When we estimated the total copy number by the overlap in its 95% CI in the scatterplot analysis, our assays clearly estimated the total copy number for each sample at 1 to 4 copies. Among the 88 JCH samples, 6 individuals (6.8%) had 1 copy, 27 (30.7%) had 2 copies, 41 (46.6%) had 3 copies, and 14 (15.9%) had 4 copies of *CYP2D6*. The copy number values obtained for the 3 assays were concordant for all samples, indicating that the entire *CYP2D6* gene had been duplicated or deleted as a unit. When we combined the results of 3 qPCR assays, we were able to obtain more precise copy number data (Fig. 1).

Among the *CYP2D6* alleles registered in the human CYP allele database, we selected 23 variants that have been reported to have functional significance for the CYP2D6 enzyme in vitro or in vivo (see Tables 2 and 3 in the online Data Supplement). We also selected 1 variant with wild-type function (2850C>T) to determine the frequency of *CYP2D6*2*. With the 88 JCH samples, we performed RETINA assays for these 24 variants and found only 7 loci to be polymorphic in our population [100C>T, 1707delT, 1758G>A, 1846G>A, 2573_2574insC, 2850C>T, and gene conversion to *CYP2D7P1* (cytochrome P450, family 2, subfamily D, polypeptide 7 pseudogene 1) in exon 9 (Ex9_2D7conv)] (Fig. 2). The other 17 RETINA assays detected no variant alleles in any of the JCH samples. The RETINA assays showed clear allelic asymmetries in the heterozygote clusters in the 100C>T, 2850C>T, and Ex9_2D7conv assays, and we observed variant alleles in 4 assays (1707delT, 1758G>A, 1846G>A, and 2573_2574insC) in 1 sample. The existence of all these variant alleles was confirmed by direct sequencing (see Fig. 4 in the online Data Supplement).

ESTIMATION OF *CYP2D6* ALLELES IN 455 JAPANESE INDIVIDUALS

We subsequently performed qPCR assays and 24 RETINA assays for 455 Japanese individuals. According to the results of 3 qPCR assays combined, we found that 42 individuals (9.2%) had 1 copy, 207 (45.5%) had 2 copies, 161 (35.4%) had 3 copies, 40 (8.8%) had 4 copies, and 5 (1.1%) had 5 copies of the *CYP2D6* gene (see Fig. 5 in the online Data Supplement). The RETINA method indicated 7 loci to be polymorphic: 260 individuals (57.1%) had a 100C>T allele, 3 (0.7%) had a 1758G>A allele, 4 (0.9%) had a 1846G>A allele, 5 (1.1%) had a 2573_2574insC allele, 122 (26.8%) had a 2850C>T allele, 4 (0.9%) had a 4125_4133dupGTGCCCACT allele, and 202 (44.4%) had an Ex9_2D7conv

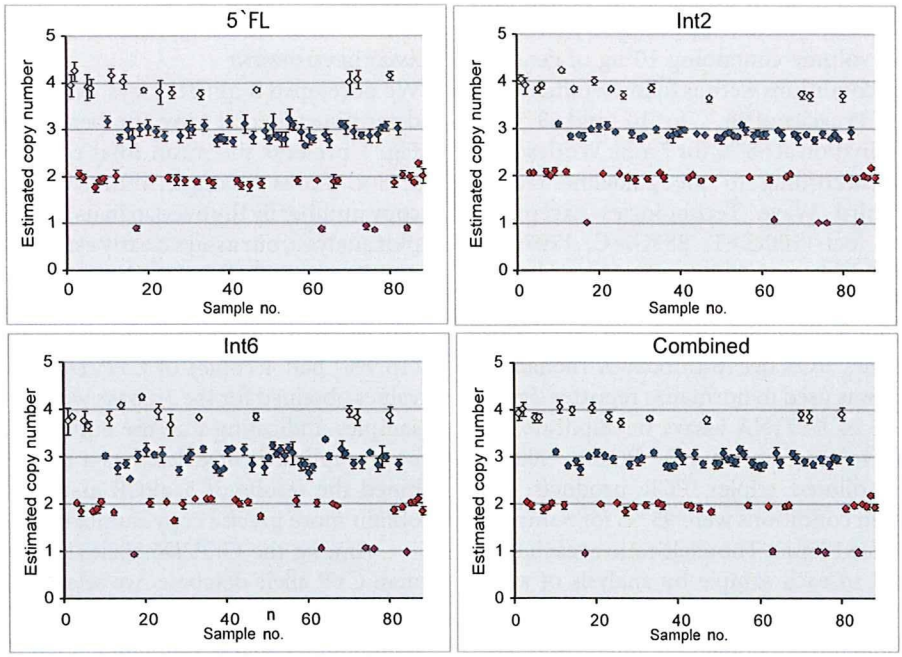

Fig. 1. Determination of total gene copy number in JCH samples.

Scatter-plot analysis views of 3 qPCR assays for the total gene copy number determination. Closed purple, red, blue, and light green diamonds indicate 1 copy, 2 copies, 3 copies, and 4 copies, respectively. Error bars indicate the 95% CI.

allele. A 1707delT allele found in 1 JCH sample was not observed in the 455 Japanese samples. These RETINA assays showed clear allelic asymmetries in the heterozygote clusters, and we determined the allele ratio of each variation in each individual. From the results obtained by qPCR and mPCR-RETINA, we determined the allele copy number at each variation locus and estimated the *CYP2D6* allele with the CNVphaser. We found 16 different types of the *CYP2D6* allele in the 455 Japanese individuals (Table 1). *CYP2D6*1*, **2*, and **10-*36* were the common *CYP2D6* alleles, and *CYP2D6*5* and **10* were relatively frequent (>5%). The frequencies of the other *CYP2D6* alleles were very low. Although whole-gene deletion (*CYP2D6*5*) and duplications could previously be detected only by long PCR or the Southern-RFLP technique, our method was able detect these variations with the allele copy number data. In addition, we also detected novel *CYP2D6* alleles, such as *CYP2D6*10-*36-*36* and **10-*10-*36*. When we compared the frequencies of *CYP2D6* alleles with those described in previous reports *(25, 26)*, the results were very similar (Table 1). In the diplotype analysis, we found various *CYP2D6* diplotypes (Table 2). *CYP2D6*1/*1* and **1/*10-*36* were the most common diplotypes (approximately 20% each) in our population; other common diplotypes (>5%) were *CYP2D6*1/*2*, **2/*10-*36*, **10-*36/*10-*36*, **1/*5*, and **1/*10*.

CONFIRMATION OF ESTIMATED *CYP2D6* ALLELES BY LONG PCR OR SOUTHERN-RFLP ANALYSIS

To confirm the estimated *CYP2D6* alleles that composed the gene deletion, duplications, or triplications, we conducted long PCR or Southern-RFLP analysis according to previously described protocols *(16, 26, 27)*. Fig. 3 shows representative results of the confirmation by the long PCR method. We detected *CYP2D6*5*-specific PCR products (6 kb in lane 3, 3.5 kb in lane 4) in individuals estimated to have *CYP2D6*5*. The duplication-specific PCR products (4.8 kb for *CYP2D6*1-*1*, **2-*2*, and **10-*10* in lane 5) were detected in individuals estimated to have these duplicated *CYP2D6* alleles. We also observed *CYP2D6*10-*36–* or **36-*36*–specific PCR products (6.4 kb in lane 5) in individuals estimated to have these *CYP2D6* alleles. For the novel triplications (*CYP2D6*10-*36-*36* and **10-*10-*36*) found in this study, we performed Southern-RFLP analysis and detected a triplication-specific fragment (54 kb) in individuals estimated to have these *CYP2D6* alleles (Fig. 4).

Discussion

Accurate determination of the functional-gene dosage of *CYP2D6* in pharmacogenetic studies is important, but presently available methods are inadequate to de-

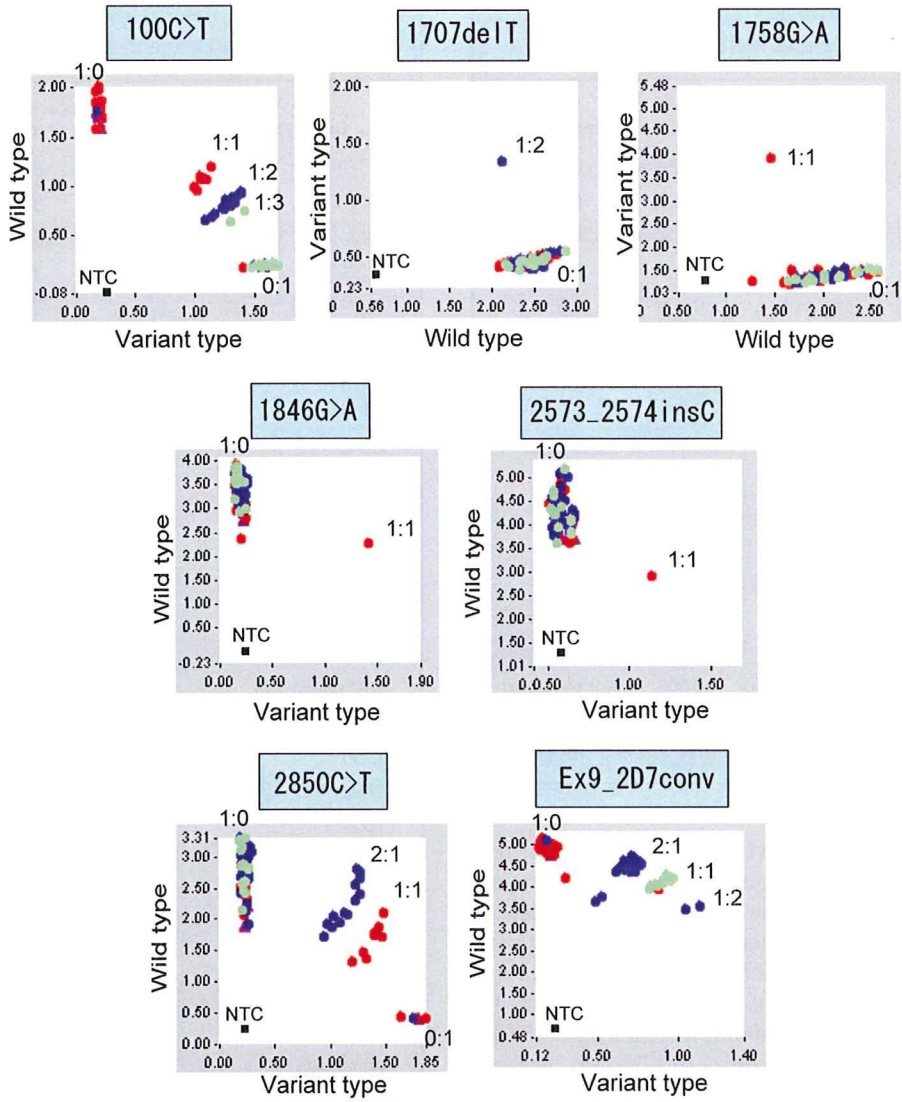

Fig. 2. Determination of allele ratio in JCH samples.

Allelic discrimination (AD) plot views in 7 RETINAs for determining allele ratio. Vertical axis of the AD plots indicates normalized FAM allele signal, and horizontal axis indicates normalized Yakima Yellow allele signal. Total gene copy numbers are indicated in the same colors as in Fig. 1. Black square indicates no template control (NTC). Numbers in AD plot indicate allele ratio, as determined by calibration curve method.

termine it. To our knowledge, our method is the first to determine the exact copy number of nonfunctional, impaired-functional, and normal-functional *CYP2D6* genes in each individual. Our genotyping method with a combination of qPCR and mPCR-RETINA was able to determine the allele copy number at each variation locus to precisely estimate the number of *CYP2D6* alleles by the CNVphaser. Furthermore, our method could detect whole-gene deletion, duplications, and previously unreported *CYP2D6* triplications without the use of the long PCR or Southern-RFLP technique. We think these characteristics are the crucial advantages of our method. We are confident that our method predicts CYP2D6 enzymatic activity more precisely and is useful for pharmacogenetic study of drugs metabolized by CYP2D6.

Although several genotyping methods have been developed for the detection of *CYP2D6* alleles, they lack a quantitative capability and cannot provide an

Table 1. *CYP2D6* allele frequencies in 455 Japanese individuals.

CYP2D6 allele	Enzyme activity[a]	455 Japanese	249 Japanese[b]
**1*	Wild type	0.434	0.456
**2*	Wild type	0.128	0.141
**4*	None	0.004	0.000
**5*	None	0.057	0.052
**10*	Impaired	0.086	0.054
**14B*	None	0.003	0.006
**18*	None	0.004	0.002
**21*	None	0.005	0.006
**44*	None	0.000	0.002
**1-*1*	Increased	0.005	0.006
**2-*2*	Increased	0.004	0.004
**10-*10*	Impaired	0.006	0.004
**10-*36*	Impaired	0.242	0.267
**10-*10-*36*	Unknown	0.002	Not examined
**10-*36-*36*	Unknown	0.013	Not examined
**36-*36*	None (negligible)	0.005	Not examined

[a] Enzyme activity is as described in the CYP allele database.
[b] These frequency data are from 2 reports by Soyama et al. *(25, 26)*.

Table 2. *CYP2D6* diplotypes in 455 Japanese individuals.

Diplotype	Probability	Individuals, n	Frequency
**1/*10-*36*	1	90	0.198
**1/*1*	1	89	0.196
**1/*2*	1	51	0.112
**2/*10-*36*	1	32	0.070
**10-*36/*10-*36*	0.96	30	0.066
**1/*5*	1	29	0.064
**1/*10*	1	26	0.057
**10/*10-*36*	0.99	21	0.046
**2/*10*	1	11	0.024
**5/*10-*36*	1	8	0.018
**2/*2*	0.97	7	0.015
**5/*10*	1	6	0.013
**2/*5*	1	5	0.011
**10/*10*	0.92	4	0.009
**1/*10-*36-*36*	1	4	0.009
**10-*36/*36-*36*	1	3	0.007
**10-*36/*10-*36-*36*	1	3	0.007
**1/*21*	1	3	0.007
**1/*10-*10*	1	3	0.007
**1/*1-*1*	1	3	0.007
**1/*2-*2*	1	3	0.007
**5/*14B*	1	2	0.004
**4/*10*	1	2	0.004
**5/*10-*36-*36*	0.62	2	0.004
**10-*36/*10-*10-*36*	0.87	2	0.004
**1/*18*	1	2	0.004
**2/*10-*36-*36*	1	2	0.004
**2/*10-*10*	0.79	2	0.004
**4/*10-*36*	1	1	0.002
**10/*18*	1	1	0.002
**10/*21*	1	1	0.002
**10-*36/*18*	1	1	0.002
**10-*36/*21*	1	1	0.002
**1/*4*	1	1	0.002
**1/*14B*	1	1	0.002
**1/*36-*36*	1	1	0.002
**1-*1/*10-*36*	1	1	0.002
**2-*2/*10*	0.84	1	0.002

exact copy number of functional *CYP2D6* genes. Duplication and multiplication of the *CYP2D6* gene are usually considered as one *CYP2D6* allele, such as *CYP2D6*1xN*, and the exact functional effect of gene dosage cannot be evaluated. In our population, 9.2% of the individuals had a loss of 1 copy of *CYP2D6*, 45.3% had more than 2 copies, and only less than half (45.5%) of our population had 2 copies of *CYP2D6*. Because different types of *CYP2D6* variation are known to affect the function of CYP2D6 activity, accurate determination of the functional-gene dosage is essential for detailed pharmacogenetic analysis of CYP2D6. At a frequency of 34.8%, *CYP2D6*10* is common in our population, but it is represented by various *CYP2D6* alleles, including *CYP2D6*10*, **10-*10*, **10-*36*, **10-*10-*36*, and **10-*36-*36*. Among the 258 individuals with *CYP2D6*10*, 86 (33.3%) possessed no *CYP2D6* gene with wild-type activity. Among these individuals, 26 had only 1 copy of *CYP2D6*10* (**10-*36/*18*, **10-*36/*21*, **10-*36/*36-*36*, **10/*18*, **10/*21*, **4/*10*, **4/*10-*36*, **5/*10*, **5/*10-*36*, and **5/*10-*36-*36*), 58 had 2 copies of *CYP2D6*10* (**10-*36/*10-*36*, **10-*36/*10-*36-*36*, **10/*10*, and **10/*10-*36*), and 2 individuals had 3 copies of *CYP2D6*10* (**10-*36/*10-*10-**36). Because differences in *CYP2D6*10* copy number are thought to affect differences in enzymatic activity *(3, 28)*, the risk of treatment failure or toxicity of drugs metabolized by CYP2D6 might be different among these individuals. We believe our method will contribute to establishing a more detailed and precise estimation of CYP2D6 enzymatic activity.

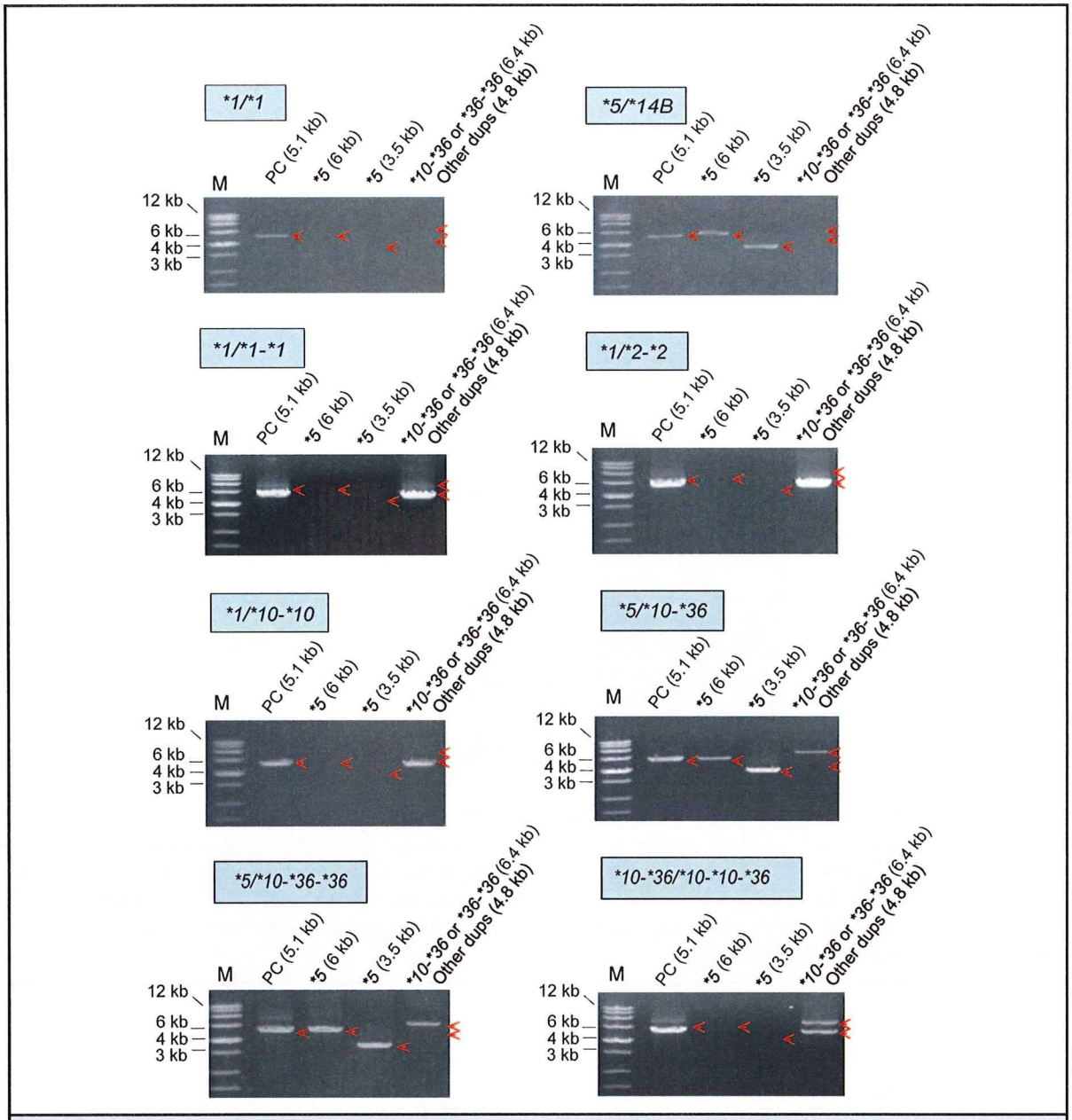

Fig. 3. Confirmation of estimated *CYP2D6* alleles by long PCR.

Estimated diplotypes of representative samples are indicated above each gel image. Sample estimated as *CYP2D6*1/*1* was used as a non-CNV control. Arrows indicate positions of specific fragments obtained by the long PCR. Lane 1, size marker (M); lane 2, 5.1-kb fragment for *CYP2D6* positive control (PC), which should be detected in all samples; lanes 3 and 4, 6-kb and 3.5-kb fragments, respectively, for samples with *CYP2D6*5*; lane 5, 6.4-kb fragment for samples with *CYP2D6*10-*36* or **36-*36* and 4.8-kb fragment for samples with other duplications (*CYP2D6*1-*1*, **2-*2*, or **10-*10*).

In addition to the advantage of quantitative capability, our method has other merits. The most critical point is the ease of the protocol with its high-throughput format. Long PCR–RFLP requires 4 steps, including long PCR, nested PCR, cleavage by restriction enzymes, and gel electrophoresis *(8)*. The AmpliChip CYP450 method requires 5 steps, including long PCR, fragmentation, labeling, hybridization, and staining *(11)*, and the SNaPshot method requires 5 steps (long PCR, purification of the PCR product,